EXPERIMENTAL EVALUATION OF VISIBLE LIGHT COMMUNICATION BASED BROADCASTING

A Thesis

by

İbrahim Bağlıca

Submitted to the
Graduate School of Sciences and Engineering
In Partial Fulfillment of the Requirements for
the Degree of

Master of Science

in the
Department of Electrical and Electronics Engineering

Özyeğin University
January 2024

Copyright © 2024 by İbrahim Bağlıca

EXPERIMENTAL EVALUATION OF VISIBLE LIGHT COMMUNICATION BASED BROADCASTING

Approved by:

Professor Murat Uysal, Advisor
Department of Electrical and Electronics Engineering
Özyeğin University

Assistant Professor Çağatay Edemen
Department of Electrical and Electronics Engineering
Özyeğin University

Professor İbrahim Altunbaş
Department of Electronics and Communication Engineering
Istanbul Technical University

Date Approved: 25 December 2023

This thesis is dedicated to my beloved parents, who have inspired me to learn and supported me in all my endeavors.

ABSTRACT

Visible Light Communication (VLC) uses light-emitting diodes (LED)s to transmit data by turning them on and off at very high speeds, too fast for the human eye to perceive. In outdoor environments, LED-based streetlights can be utilized as VLC transmitters. Given the ubiquity of streetlights, they are particularly useful for outdoor broadcasting as required in public safety systems. In this thesis, we develop an FPGA-based VLC system with on-off keying using an LED-based streetlight. The system is built upon the Eclypse Z7 FPGA platform integrated with opto-electronic transmitter and receiver front ends. We present bit error rate (BER) and signal-to-noise ratio (SNR) performance results in indoor and outdoor environments, at various transmission distances.

ÖZETÇE

Görünür Işıkla haberleşme (VLC) ışık yayan diyotları (LED'leri) kullanarak veri iletmek için kullanılır. LED'ler çok yüksek hızlarda açılıp kapatılarak veri iletilir, ancak insan gözü bunu algılayamaz. Açık hava ortamlarında, LED tabanlı sokak lambaları VLC vericileri olarak kullanılabilirler. Sokak lambalarının yaygınlığı göz önüne alındığında, özellikle kamu güvenliği sistemlerinde gerektiği gibi tüm alıcılara aynı anda bilgi aktarma için oldukça faydalıdırlar. Bu tezde, LED tabanlı bir sokak lambası kullanarak aç-kapa anahtarlama yöntemiyle FPGA tabanlı bir VLC sistemi geliştiriyoruz. Sistem, opto-elektronik verici ve alıcı ön uçları ile entegre Eclypse Z7 FPGA platformu üzerine inşa edilmiştir. Çalışmamızda farklı iletim mesafelerinde iç mekan ve dış mekan ortamlarında bit hata oranı ve sinyal gürültü oranı başarım sonuçları sunulmuştur.

ACKNOWLEDGEMENTS

I would like to express my appreciation to my advisor, Prof. Murat Uysal. It has been a pleasure to work with him as a master's student and as a research assistant and I would like to thank him for his wisdom, friendship, encouragement, support, patient guidance, invaluable insights, and suggestions during this experience. Without his constant support and guidance, the thesis would not have been possible. I also had the honorable opportunity to work with him. I learned a lot from him throughout my master's studies.

I would like to express my sincerest gratitude to the members of my thesis committee, Prof. İbrahim Altunbaş and Assistant Prof. Çağatay Edemen, for their service on my committee and their careful review of my thesis.

I acknowledge with sincere thanks the funding I received for my master's from the Turkish Scientific and Technological Research Council (TÜBİTAK) under Grant 121N006 (sub-grant of 120N573).

I am also grateful for the technical and non-technical discussions I had with my colleagues at The Center of Excellence for Optical Wireless Communications Technologies (OKATEM), including Görkem Mutlu, Sude Ergin, Anılcan Tosun, Batuhan Başar, Muhammet Emin Akbulut, Burak Kebapçı, Bismillah Nasir Ashfaq, Abdülkerim Çekinmez, Samet Yıldız, and Assistant Prof. Mohammed Elamassie, for their assistance during my studies at Özyeğin University. The collaboration and the fruitful conversations with CT&T members have also been a source of enjoyment for me

My sincere gratitude goes out to my parents, Ali and Sultan, who have always supported me unconditionally throughout my life. They have made great sacrifices. My heartfelt thanks go out to Sude for her boundless kindness, unrestrained love, and unlimited patience. I would like to thank my sisters and brother, Neslihan, Tuğba, and Mustafa for their continuous support. The unwavering trust and willingness of my family to endure the difficulties and stresses of my endeavors will forever be a debt I hold close to my heart. My final thanks go to Murphy, my wonderful dog.

ACRONYMS

AC	Alternating Current
ADC	Analog-to-Digital
APD	Avalanche Photodiode
APSoC	All Programmable System-on-Chip
ASIC	Application-Specific Integrated Circuit
AXI	Advanced eXtensible Interface
AWGN	Additive White Gaussian Noise
BER	Bit Error Rate
BRAM	Block Random Access Memory
BJT	Bipolar Junction Transistor
CCD	Charge-Coupled Device
cd	Candela
CMOS	Complementary Metal Oxide Semiconductor
CRI	Color Rendering Index
DAC	Digital-to-Analog
DC	Direct Current
EDRS	European Data Relay System
EPC	Efficient Power Conversion
ESA	European Space Agency
FET	Field-Effect Transistor
FPGA	Field Programmable Gate Array
FR	Flame Retardant
GaN	Gallium Nitride

Gb/s	Gigabits Per Second
GaAs	Gallium Arsenide
GPIO	General Purpose Input/Output
IDE	Integrated Design Environment
I/O	Input/Output
ILA	Integrated Logic Analyzer
IoT	Internet of Things
I2V	Infrastructure-to-Vehicle
IR	Infrared
IP	Internet Protocol
JPL	Jet Propulsion Laboratory
K	Kelvin
LCRD	Laser Communication Demonstration
LED	Light Emitting Diode
lm	Lumen
LMM	Linear Mode Modulator
LOS	Line of Sight
MIT	Massachusetts Institute of Technology
MAC	Media Access Control
Mb/s	Megabits Per Second
MS/s	Megasample Per Second
MC	Modulator for Communication Stage
MDC	Management Data Clock
MDIO	Management Data Input/Output
MLCD	Mars Laser Communications Demonstration
MOSFET	Metal-Oxide-Semiconductor Field-Effect Transistor
MS/s	Mega-Symbols Per Second

NEP	Noise Equivalent Power
NLOS	Non-Line of Sight
OFDM	Orthogonal Frequency Division Multiplexing
OOK	On-Off Keying
OWC	Optical Wireless Communication
PC	Power Control Stage
PCB	Printed Circuit Board
PFC	Power Factor Correction Stage
PLC	Powerline Communication
PIC	Peripheral Interface Controller
PL	Programmable Logic
PMT	Photomultiplier Tube
PS	Processing System
PSM	Parallel Switch Mode
RAM	Random Access Memory
RIS	Reconfigurable Intelligent Surface
RF	Radio Frequency
RGMII	Reduced Gigabit Media Independent Interface
RM	Ripple Modulation
RX	Receiver
SDK	Software Development Kit
SDR	Software-Defined Radio
SILEX	Semiconductor Inter-Satellite Laser Experiment
SMA	SubMiniature version A
SM	State Machine
SMM	Switching Mode Modulator
SNR	Signal-to-Noise Ratio

SoC System-on-Chip

SSM Series Switch Modulator

S2P Streetlight-to-Pedestrian

S2V Streetlight-to-Vehicle

TX Transmitter

VLC Visible Light Communication

UAV Unmanned Aerial Vehicle

UDP User Data Protocol

USRP Universal Software Radio Peripheral

UV Ultraviolet

TABLE OF CONTENTS

LIST OF TABLES

LIST OF FIGURES

CHAPTER I

INTRODUCTION

1.1 Motivation

A rapidly advancing world demands innovative solutions to meet the demands of evolving urban landscapes. As such, streetlight VLC broadcasting demands our attention, poised to revolutionize urban lighting and communication. The innovative concept seamlessly integrates VLC technology into conventional streetlights, allowing seamless data communication between devices and illuminating the streets. In addition to improving the quality of life for residents and visitors alike, streetlight VLC broadcasting can transform cities into smart, interconnected hubs.

The remarkable improvement in connectivity offered by streetlight VLC broadcasting is one of its most notable advantages. In addition to creating an extensive network of data transmission points throughout the city, VLC technology leverages the existing streetlight infrastructure. In addition to providing faster, more reliable communication and access to information, this enhanced connectivity allows citizens, businesses, and public services to work more efficiently and productively.

In addition, streetlight VLC broadcasting will advance public safety to new heights. Emergency services, law enforcement, and city officials can communicate seamlessly through the real-time data exchange enabled by VLC technology. In emergencies, this capability results in faster response times, more efficient traffic management, and proactive safety measures for residents and visitors. Using streetlight VLC broadcasting, cities can monitor traffic flow and crowd density and make informed decisions based on collected data.

Streetlight VLC broadcasting is a critical building block in the foundation of smart cities as they evolve and embrace the concept. This innovative technology empowers cities to become more efficient, responsive, and sustainable. In addition to smart parking, waste management, environmental monitoring, and public Wi-Fi, streets serve as an interconnected data exchange ecosystem.

In summary, streetlight VLC broadcasting aims to revolutionize urban living, creating more innovative, safer, and environmentally friendly cities. The streetlight VLC broadcasting network illuminates the path to a future where technology and sustainability converge to benefit citizens of all cities as they grow and adapt to the challenges of the digital age.

1.2 Overview of Streetlight Wireless Communication

Innovative technologies enable streetlights to communicate with each other, making them intelligent and interconnected. Urban environments benefit greatly from this innovative approach because they can wirelessly exchange data and connect with other smart city devices.

Streetlight communication has the following key benefits:

- **Energy Efficiency:** Streetlight communication allows individual lights or communities to be monitored and controlled in real-time. Through this level of control, cities can optimize energy consumption and reduce electricity costs by adjusting lighting levels based on specific conditions and needs. In order to improve overall energy efficiency, lights can be dimmed during low-traffic hours or brightened upon detecting movement.

- **Safety and Security:** Urban areas are safer due to the intelligent network of streetlights. With advanced sensors, pedestrians and motorists can be alerted to hazardous situations, such as accidents or criminal activities, and the lighting intensity can be increased automatically.

- **Traffic Management:** A traffic management system can be integrated with streetlight communication to increase traffic flow and reduce congestion. Traffic patterns are analyzed, traffic jams are detected, and the network's signal timings are dynamically adjusted to alleviate bottlenecks and optimize transportation efficiency.

- **Environmental Impact:** Streetlight communication reduces greenhouse gas emissions and the overall impact of city lighting by optimizing energy consumption. Solar panels are being used to power streetlights to promote sustainability even further, enabling them to be powered by renewable energy sources.

- **Real-Time Data Insight:** Streetlights generate a wealth of data in real-time using their interconnected devices. The collected data can be used to determine foot traffic patterns, air quality levels, and noise levels in cities. In order to develop data-driven policies for urban development, city planners can use this information to inform decision-making.

The following technologies are used in streetlight communication:

- **Radio Frequency (RF)** Streetlights and other devices communicate wirelessly using RF. With it, large urban areas can be reliably connected over radio frequencies that allow seamless data exchange.

- **Powerline Communication (PLC):** Streetlights and other connected devices can exchange data using PLC. Cost-effective connectivity options are provided without the need to invest in additional infrastructure.

- **VLC:** In VLC, data is transmitted between devices using visible light. LED streetlights can encode and transmit data by modulating their intensity, serving as illumination and communication devices.

- **Internet of Things (IoT):**A smart network of streetlights is enabled through IoT integration, in which devices and sensors are interconnected to form an intelligent system. By collecting and exchanging data, IoT-enabled devices make the system dynamic and responsive to changes.

- **Cloud Computing and Data Analytics:** A cloud-based system is often used to store and process the data collected from streetlight communication networks. Cities can extract valuable insights from large amounts of data generated with the help of data analytics.

Table 1: Comparison of wireless technologies for streetlight communications.

	Advantages/Benefits/Facts	Disadvantages/Limitations
RF	-Reliable wireless communication. -Covers large urban areas.	-Limited bandwidth, may face interference. -Potential security vulnerabilities.
PLC	- Utilizes existing power lines for connectivity. - Cost-effective infrastructure deployment. - Easy integration with power distribution systems.	- Limited data transfer rates. - Susceptible to noise and signal attenuation. - May not be suitable for remote or rural areas.
VLC	- High-speed data transfer using light signals. - Energy-efficient as it uses LED streetlights. - No additional radio frequency interference.	- Line-of-sight communication required. - Limited range compared to RF or PLC. - Obstructions can disrupt communication.
IoT	- Enables a dynamic and interconnected network. - Real-time data collection and analysis. - Enhances overall system intelligence.	- Data privacy and security concerns - Requires robust and scalable IoT infrastructure. - Potential complexity in managing a large number of devices.
Cloud	- Centralized data storage and processing. - Scalable and flexible infrastructure.	- Dependence on internet connectivity. - Data management and storage costs.

After comparing wireless technologies for streetlight communication, we chose VLC because it can transfer data at high speeds over light signals, making communication between devices efficient and rapid. Further, VLC reduces energy consumption and operational costs thanks to using LED streetlights for data transmission. Light confinement ensures that data is only transmitted within Line of Sight (LOS), thereby further enhancing security.

1.3 Overview of Optical Wireless Communication

An optical wireless communication Optical Wireless Communication (OWC) uses a visible, infrared Infrared (IR), and ultraviolet Ultraviolet (UV) band carrier to transmit unguided propagation signals in unguided media [1]. The history of OWC can be defined as signals sent through signal fires, fumes, flags of ships, and semaphore telegraphs [2]. Long-distance signaling has been used with sunlight since very early times. In ancient Greece and Rome, polished shields were used to reflect sunlight during battles to send signals [3].

As a transmitter, OWC uses lasers or LEDs. Massachusetts Institute of Technology (MIT) used a light-emitting Gallium Arsenide (GaAs) diode. As a result, they developed an experimental OWC. Through this experiment, they were able to transmit signals for television over distances exceeding 25 miles in 1962. Lasers were envisioned as being deployed primarily at OWC after the invention of the laser, and many trials were conducted there [1].

As recently as July 1960, scientists at Bell Labs utilized a ruby laser to cover a distance of 25 miles by transmitting signals, a few months later initial public announcement of a functional laser [4]. An exhaustive list of OWC demonstrated various lasers and modulation schemes between 1960 and 1970 [5]. Due to the significant divergence of laser beams and the incapacity to offset atmospheric effects, outcomes were generally unsatisfactory. During the 1970s, low-loss fiber optics became the preferred transmission media for long-distance optical transmissions, replacing OWC systems.

A research program called Semiconductor Inter-Satellite Laser Experiment (SILEX) was launched in the mid-1980s by the European Space Agency (ESA) to implement OWC for establishing laser connections between satellites. SPOT-4 is a French satellite designed for Earth observation, positioned in a sun-synchronous low orbit above the Earth's surface, and ARTEMIS geostationary satellite successfully established a 50 Megabits Per Second (Mb/s) OWC link in 2001 [6]. Reaching sequence data rates in Gigabits Per Second (Gb/s) was made possible by introducing coherent modulation techniques. [7–9]. In the current state of development, the European Data Relay System (EDRS) [10] sends and receives signals from and to non-fixed satellites, spaceships, and stationary earth stations. Space-to-ground links are based on Ka-band links between satellite communications and the OWC inter-satellite links for inter-satellite communications. For profound space applications, NASA's Jet Propulsion Laboratory (JPL) and ESA have considered optical communication between a spacecraft and Earth. It is designed to showcase optical communication from Mars to Earth with data rates ranging from 1 to 10 Mb/s, as a part of the Mars Laser Communications Demonstration (MLCD) [11]. As a part of the Laser Communication Demonstration (LCRD) program, NASA intends to showcase the implementation of OWC links for communication between satellites and from Earth to satellites, commencing in 2017 [12].

1.4 Overview of Visible Light Communication

VLC is a wireless communication technology that uses a visible portion of the electromagnetic spectrum (i.e., wavelengths of 380-750 nm) to transmit information [13]. Hence, utilizing VLC makes it feasible to repurpose the current lighting infrastructure for communication needs. In addition to high data rates and wide bandwidth, VLC has low latency and electromagnetic interference, low power consumption, and the availability of the unlicensed visible light spectrum [14]. The idea behind VLC is to use LEDs to transmit data by turning them on and off at very high speeds, too fast for the human eye to perceive.

These changes in light intensity can then be detected by a receiver, such as a photodiode, and decoded to extract the transmitted information.

Barrier penetration, reliability, and transmission distance limitations are challenges for VLC. As a result of environmental obstacles, signals can be attenuated or distorted, compromising communication reliability. VLC systems generally have a limited transmission distance due to the shorter wavelengths of visible light.

Despite these challenges, VLC has a wide variety of applications. It is suitable for rapid data transmission in enclosed spaces such as offices, hospitals, and retail stores. VLC can also be employed for indoor positioning systems, leveraging the precise control of light to determine the location of objects or individuals in closed environments. Additionally, VLC is relevant in industrial environments where RF signals might cause interference with delicate equipment or pose a safety risk. VLC has been extensively studied for indoor use cases [15] and later applied to outdoor environments [16]. In particular, VLC has been studied for vehicular applications where headlights and taillights are used for data exchange among vehicles.

1.5 Overview of Outdoor VLC

LED-based streetlights can be further utilized in outdoor environments as VLC transmitters. Given the ubiquity of streetlights, they are particularly useful for outdoor broadcasting as required in public safety systems. They can also serve as wireless hot spots for pedestrians and passing vehicles. Outdoor lights with specific illumination requirements have radiation patterns that obviously differ from their indoor counterparts.

In particular, LED luminaires for road lighting are designed to minimize light pollution, increase comfort and visibility for drivers and pedestrians, and maximize efficiency by directing light to the appropriate area of the road. Under such design constraints, their radiation patterns differ from their indoor counterparts [17, 18]. Based on non-sequential ray tracing simulations, Eldeeb et al. consider two-lane highway roads with light poles on both sides and uniformly separated from each other [19]. The mentioned studies discuss the impact of the asymmetrical pattern of streetlights on the channel characteristics without providing explicit mathematical formulas or models for calculating path loss in the Infrastructure-to-Vehicle (I2V) communication scenario [20–22]. In order to analyze streetlight-based VLC transmission, they derive a closed-form expression for the probability distribution function for the path loss. In [23], relay-assisted handover is proposed for vehicular visible light communication networks where streetlights are regarded as access points. Bette et al. present a study of outdoor VLC communication scenarios that evaluates the performance of a streetlight VLC system. The study incorporates the realistic radiation pattern of a streetlight in the simulation studies to obtain accurate estimates of the system performance [24].

In addition to the theoretical and simulation studies for outdoor VLC systems, some experimental studies were carried out. For example, to transmit identification codes for LED streetlights to cameras equipped with cameras, Trong et al. use an LED streetlight and two rolling shutters Complementary Metal Oxide Semiconductor (CMOS) sensors by installing the experimental setup in an office environment [25]. A significant impact of energy efficiency in lighting applications is the reduction of energy consumption. Depending on actual needs, streetlight brightness can be dimmed. In addition, different lighting classes can be activated based on street activity. In [26], Knobloch analyzed the simulation model and conducted an experiment with appropriate improvements in channel gain to properly street lighting while it supports VLC. He further investigated the effect of dimming and aperture on VLC performance [27]. In [28], another outdoor VLC experiment was carried out and data transmission up to 240 cm was demonstrated under different light intensities.

1.6 Thesis Outline

Most of the existing experimental works in the literature depend on laboratory equipment and off-line signal processing. In this thesis, we develop an Field Programmable Gate Array (FPGA)-based VLC system with On-Off Keying (OOK) using a LED-based streetlight. For this purpose, we use Eclypse Z7 [29] platform which features Analog-to-Digital (ADC) and Digital-to-Analog (DAC) extension boards. At the transmitter, the Processing System (PS) part of the FPGA consists of User Data Protocol User Data Protocol (UDP) server where the packets are fed from the external network. As soon as a packet arrives, it transfers that packet to the Programmable Logic (PL) part of the FPGA through the Advanced eXtensible Interface (AXI) bus between PL and PS parts. The PL modulates the signal and feeds the LED driver. After the transmitted signal goes through the propagation medium, it is collected by a photodetector. A narrow-band optical filter is used to prevent saturation and reduce environmental light noise. The analog output signal from the photodetector is digitalized using ADC and fed to the demodulation block in the FPGA. Finally, the received package is transferred to a previously defined Internet Protocol (IP) address through Ethernet.

The remainder of this thesis is as follows

1. In the first part of the thesis, we will explain the hardware components for streetlight VLC broadcasting. Following that, we will compare these products within their classes. Firstly, we will describe and compare the various lights used in street lighting. As the next step, we will discuss LED drivers for VLC. Next, we will introduce the devices that control the communication environment. Finally, we will compare photodetectors for the receiver front end.

2. In the second part of this thesis, we will explain the system architecture we developed for experimental demonstration. Next, we will explain the LED driver design, an essential part of the transmitter's front end. Following that, we will introduce the

system's receiver front end. Then we discuss implementation issues on FPGA the transmitter and receiver blocks.

3. In the third part of the thesis, we discuss photometric quantities for streetlights. Next, we provide our performance measurement results.

1.7 Organization

The thesis is organized as follows. Chapter 2 focuses on the hardware selection for streetlight VLC broadcasting. Chapter 3 focuses on the experimental demonstration of VLC broadcasting. Chapter 4 focuses on the measurement results. These chapters are organized as follows:

- Chapter 2 has four sections. In Section 2.1 on page 13, we discuss and compare the technologies used in streetlights. In Section 2.2 on page 20, we explain VLC LED structure and we discuss and compare modulator types. In Section 2.3 on page 25, we discuss and compare controllable transceivers for communication systems. In Section 2.4 on page 29, we discuss and compare photodiodes for the receiver front end.

- Chapter 3 has four sections. In Section 3.1 on page 39, we present the overall system architecture. In Section 3.2 on page 40, we design an LED driver for the transmitter's front end. In Section 3.3 on page 43, we present the receiver's front end. In Section 3.4 on page 44, we explain FPGA implementation for transmitter and receiver.

- Chapter 4 has four sections. In Section 4.1 on page 55, we discuss photometric quantities for streetlights, and we measure the streetlight that is used for experimental demonstration. In Section 4.2 on page 58, we present the bandwidth for our streetlight. In Section 4.3 on page 59, we present BER performance and the impact of the matched filter in experiments conducted in the laboratory environment. In Section 4.4 on page 68, we present SNR performance while BER is zero conducted in the outdoor environment.

CHAPTER II

HARDWARE COMPONENTS SELECTION

In this chapter, we discuss the hardware components for streetlight VLC broadcasting. Following that, we compare these products within their classes. Firstly, we describe and compare the various lights used in street lighting. As the next step, we will discuss LED drivers for VLC. Next, we introduce the devices that control the communication environment. Finally, we discuss and compare photodetectors for the receiver front end.

To deploy outdoor VLC systems successfully, hardware selection is crucial. Several factors need to be considered to ensure that outdoor communication is reliable and efficient, such as the type of drivers, transmitters and receivers, and optical components. Outdoor VLC systems can work over longer distances outdoors by carefully selecting hardware components and system designs to overcome ambient light and interference variations.

Following is the remainder of this chapter. In Section 2.1, we discuss and compare the technologies used in streetlights. In Section 2.2 on page 20, we explain VLC LED structure and we discuss and compare modulator types. In Section 2.3 on page 25, we discuss and compare controllable transceivers for communication systems. In Section 2.4 on page 29, we discuss and compare photodiodes for the receiver front end.

2.1 Streetlights

Streetlighting is crucial to illuminating roads and surrounding areas in urban and residential settings at night. The purpose of these lights is to enhance traffic safety, ensure visibility for pedestrians and drivers, and reduce crime. Moreover, they facilitate social activities at night and promote energy efficiency using innovative lighting technologies. A lamp or fixture is commonly used for street lighting. In the past, gas-discharge lamps, like mercury vapor lamps, sodium vapor lamps, and metal halide lamps, were used to illuminate large areas with high-intensity light. Nevertheless, these lamps may exhibit a lower energy efficiency and be limited in lifespan.

Lighting for streets and roads has been revolutionized by LED technology in recent years. Compared to conventional lamps, LEDs have a longer lifespan and are more energy efficient. LEDs' flexibility in controlling color temperature and lighting level is a significant advantage. As a result, user customization and environment adaptation are improved.

A street or road light configuration can be determined by traffic flow, the environment, and its intended purpose. In contrast, residential areas favor gentler and subdued lighting, whereas main thoroughfares require brighter and more intense illumination. As well as choosing the right fixtures and lenses, it is essential to prevent unnecessary light pollution and ensure proper light direction.

As a result, street and road lighting enhances safety and supports urban social life. With the shift towards LED technology, lighting systems continue to evolve, focusing on energy efficiency, environmental impact, and aesthetic considerations.

2.1.1 Low-Pressure Sodium Vapor Lamps

Gas-discharge lamps, such as low-pressure sodium vapor lamps, are widely used within the lighting industry. Low-pressure ionization of sodium vapor produces yellow light. These lamps provide several advantages, including their energy efficiency, long lifespan, and high efficacy.

A glass tube contains a small amount of sodium metal and argon gas. High energy is created when sodium atoms are highly energized when electricity passes through the tube. Within this low-pressure environment, energized sodium atoms transition to lower energy levels and emit yellow light.

There are several benefits of low-pressure sodium vapor lamps, including long lifespans, high efficiency, low energy consumption, and good color rendering. Low power consumption makes them a popular street lighting option that reduces energy costs. Furthermore, these lamps have a long lifespan, so maintenance costs can be reduced.

Despite their advantages, these lamps have limitations, particularly when it comes to color rendering. Their yellowish light makes them less suitable for applications requiring precise color representation due to their limited ability to render colors accurately. A short warm-up period may be required to achieve the maximum brightness from these lamps.

Figure 1: Low-Pressure Sodium Vapor lamp.

2.1.2 High-Pressure Mercury Vapor Lamps

Gas-discharge lamps with high-pressure mercury vapor are commonly used in the lighting industry. Mercury vapor is ionized at high pressure to produce bright, white light. In addition to their energy efficiency and long lifespan, these lamps provide excellent color rendering. Under high pressure, mercury vapor is contained in glass tubes. Electricity ionizes mercury atoms when applied to the lamp, causing them to become highly energized. A bright white light is produced as these energized mercury atoms return to their lower energy levels.

The benefits of high-pressure mercury vapor lamps include high illumination, energy efficiency, and a long lifespan. Lighting for streets, stadiums, and industrial applications is common use for them. Moreover, they have good color rendering, making them suitable for applications requiring accurate color representation.

There are, however, some limitations to high-pressure mercury vapor lamps. The recycling process involves challenges related to heat dissipation, brightness control, and the environmental impact of mercury use. Furthermore, these lamps may need some time to warm up before they reach their full brightness.

Figure 2: High-Pressure Mercury Vapor Lamp.

2.1.3 Metal Halide Lamps

Gas-discharge lamps, such as metal halide lamps, are commonly used in various applications. In order to produce a bright white light, a gas mixture that contains metal halide compounds is ionized. Extended lifespans, excellent color rendering, and high efficiency distinguish these lamps.

The metal halide lamp interacts with the gases within a glass tube through an electric arc. A metal halide compound in the gas mixture becomes energized by passing an electric current. A high-energy state is converted into white light using phosphor-coated glass tubes.

There are several benefits to using metal halide lamps. Besides being highly efficient, they have a long lifespan, provide accurate color rendering, and offer various color options.

With their high light output, these lamps can effectively illuminate large areas. Consequently, they are common in photography studios, stage lighting setups, sports arenas, and industrial facilities that require accurate color reproduction.

There are, however, some limitations to metal halide lamps. In addition to their high initial costs, they require a long warm-up time before their full brightness is reached. Specific models may also have issues with cooling periods and color consistency.

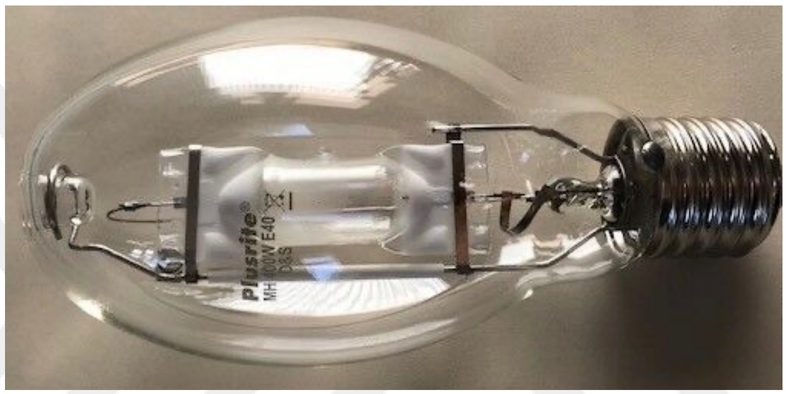

Figure 3: Metal Halide lamp.

2.1.4 LED Technology

Lighting has been revolutionized by LED technology. A semiconductor material emits light when an electric current passes through it. Compared to traditional lighting sources, this technology offers numerous advantages. LEDs have some key features and benefits:

1. **Energy Efficiency:** A LED's energy efficiency allows it to convert electrical energy into light more efficiently, which reduces energy consumption and increases light output. The result is a reduction in energy costs and an improvement in environmental sustainability.

2. **Long Lifespan:** The average LED lifetime is between 25,000 and 50,000 hours. In addition to reducing the frequency of replacement, their longevity reduces maintenance costs.

3. **Rapid Startup and Response Time:** LEDs respond quickly to input changes and reach full brightness instantly. They are more energy efficient with faster startup times and flicker-free illumination than other lighting options.

4. **Color options and Control:** LEDs can be controlled to produce a wide range of colors and can reproduce accurate colors. A further benefit of these lights is that they can be adjusted for color temperature and brightness, allowing for greater flexibility in lighting design.

5. **Durability:** LEDs are highly durable and shock and vibration resistant. In contrast to traditional bulbs, these bulbs do not contain fragile components like glass or filaments, so they are more resistant to external damage.

6. **Environmental Friendliness:** LEDs consume little energy and generate minimal waste, so they are considered environmentally friendly. Mercury and lead are not present in them, so potential environmental hazards are reduced.

As a result of these exceptional features and advantages, LEDs have become the preferred choice for a wide variety of lighting applications. Among the many applications for which they are used are residential, commercial, street, automotive, and industrial lighting. In addition, LED technology continues to improve efficiency, color quality, and application possibilities.

Figure 4: LED streetlight.

Comparisons of key specifications, limitations, and advantages of different lighting technologies are presented in the following Table 2. Understanding the characteristics of these lighting technologies can help make informed choices for lighting solutions. Several factors need to be considered regarding efficiency, Color Rendering Index (CRI), lifespan, start-up time, dimming capability, environmental impact, maintenance requirements, heat emission, size, flexibility, and cost outlined in Table 2.

Table 2: Comparison of light sources.

	Low-Pressure Sodium Lamps	**High-Pressure Mercury Lamps**	**Metal Halide Lamps**	**LEDs**
Efficiency	High	Moderate	Moderate to high	Very high
CRI	Very low	Moderate	Moderate to high	High
Lifespan	Long	Moderate to long	Moderate to long	Long
Start-up Time	Long	Long	Moderate	Instantaneous
Flexibility	Limited	Limited	Limited	High
Cost	Moderate to low	Moderate	Moderate to high	High
Dimming	Limited	Limited	Moderate	Excellent
Size	Bulky	Bulky	Moderate	Compact

Ultimately, LED streetlights are the ideal choice for implementing VLC in streetlighting systems since they are fast and controllable, which makes them ideal for transferring data.

2.2 VLC LED Driver

In terms of VLC LED drivers, they are electronic devices or circuits designed to drive and control LEDs in VLC applications to transmit information by visible light. An essential function of this device is to facilitate the transmission of data over a medium based on visible light.

2.2.1 VLC Driver Structure

As shown in Figure 5, a schematic representation of a VLC LED driver can be seen, divided into the following three stages.

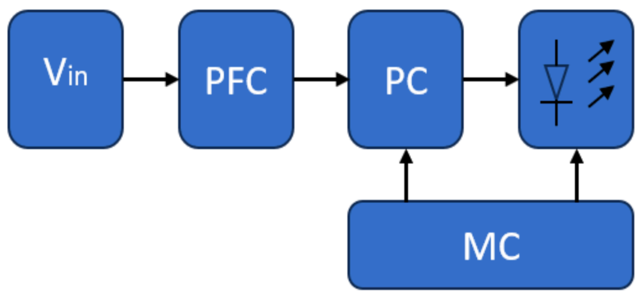

Figure 5: Schematic representation of a VLC LED driver [30].

- **Power Factor Correction Stage (PFC):** The initial block rectifies the Alternating Current (AC) grid voltage, ensuring that the current drawn from the grid adheres to energy quality standards ensures it is subjected to very minimal distortion. The criteria are highly restrictive for lighting devices with a power exceeding 5 watts. [30, 31].

- **Power Control Stage (PC):** The purpose of this block is to adjust or regulate the LED's Direct Current (DC) voltage or current levels to ensure they correspond to those required by the next block. This type of converter is typically a step-up or step-down converter, capable of regulating the supply voltage and filtering the residual low-frequency ripples in the voltage supply provided by the PFC block. Furthermore, this block can also be used to dim the lights [30].

- **Modulator for Communication Stage (MC):** It is this extra block that is added to a conventional LED driver in order to add VLC functionality to it. As a result of a voltage or current shaping process, the VLC LED stimuli can be produced to obtain the VLC LED stimuli. According to the type of modulation and bandwidth requirements that have to be met by this block, as well as other aspects such as cost, circuit complexity, and efficiency, the circuit topology of this block is defined. However, there is no need to include all of these blocks in every VLC system because not all are required. An LED driver that runs on batteries will omit a PFC stage, for example, when it operates on batteries. Likewise, it is not required that circuit blocks be separated, e.g., an integrated power stage may perform two functions simultaneously in a single stage [30, 32].

2.2.2 Modulator Types

1. **Linear Mode Modulator (LMM):** The topologies of these devices are based on the fact that transistors operate within a linear region of their operation. It is common to find amplifiers in classes A, B, AB, and C. A class C amplifier, in particular, can also be used as a narrowband amplifier. For a transistor to maintain the required operating point, there has to be a considerable voltage across its power terminals simultaneously with a main current flow in order for the transistor to operate on a dissipative principle, which means that to maintain the desired operating point, it needs a significant voltage across its power terminals. As a result, this type of modulator is typically inefficient in terms of energy efficiency compared to other modulators. In various applications, such as RF amplifiers and other devices, these circuits can fine-tune the output signal without imposing any distortions or shape limitations other than a typical bandwidth limitation [30].

2. **Switching Mode Modulator (SMM):** It is based on the fact that these converters utilize transistors operating in the saturation or cutoff region to generate square waveforms, which are then processed by an LC bandpass filter or a low-pass filter. It is evident that a low-pass filter-based modulator, in this sense, is better suited for VLC applications than a class D circuit because it can provide the constant bias current and the ability to modulate the current. In order to attenuate the higher harmonics of the switching frequency, the low-pass-filter-based modulator is designed to allow the communication signal to be applied to the LED while still applying the signal to the LED. In addition to lowering conduction losses, its operation provides higher efficiency [30].

   A filter's passband bandwidth depends on the switching frequency, while the DC level determines the average illumination. There are two ways to operate switching mode modulators.

   A. Average Current Control: This technique involves modulating the duty cycle (D) [33–36] to track the reference of the VLC signal, whose harmonic content remains within the passband of the filter.

   B. Ripple Modulation (RM): This technique takes advantage of the residual frequency content of the converter after filtering. It can be achieved by controlling the frequency [37] or phase [38–41] of the switching signal according to the information to be transmitted. Hence, the signal bandwidth can be exceeded with this scheme. The filter parameters, however, directly affect the resulting signal shape in this case.

3. **Series Switch Modulator (SSM):** This modulator turns on and off LEDs by using a series switch. Power control regulates the instantaneous current level, which this circuit cannot control. A single transistor, such as a Bipolar Junction Transistor (BJT)

or Metal-Oxide-Semiconductor Field-Effect Transistor (MOSFET), serves as the actuator. Unlike LMMs, this modulator does not require transistor bias currents. Transistors operate in cutoff and saturation regions as open and closed switches, respectively. Therefore, the signal modulation space for this circuit is limited to rectangular pulses. The LED p-n junction can be swept out of its remaining electrical carriers during the turn-on process using an additional switch. Therefore, the modulation bandwidth increases, and the turn-off time decreases [42, 43].

4. **Parallel Switch Mode (PSM):** It works by providing constant current to the LED through a switch connected parallel to it, which can switch the current. The current through the LED is interrupted when the switch is turned on. Thus, it can reproduce binary pulse modulation schemes with only ON/OFF levels. Since the switch loses power during shunting, this solution offers lower efficiency [33].

As shown in Table 3, each modulator type possesses critical characteristics, such as modulation method, efficiency, linearity, power dissipation, bandwidth, complexity, cost, and application. A LMM operates analog mode, offering high linearity but lower efficiency than a SMM. SMMs are digital devices with high efficiency and wide bandwidth in power supplies and converters.

Digital switching techniques are employed in SSMs and PSM modulators for high efficiency and wide bandwidth. However, they differ in their complexity and applications. A series switch modulator is suitable for DC-DC converters, while a parallel switch modulator is suitable for power supplies and converters.

Table 3: Comparison of modulators.

	Linear Mode Modulator	**Switching Mode Modulator**	**Series Switch Modulator**	**Parallel Switch Mode**
Efficiency	Lower	Higher	Higher	Higher
Modulation Method	Analog	Digital	Digital	Digital
Linearity	High	Moderate to High	High	High
Power Dissipation	Higher	Lower	Lower	Lower
Bandwidth	Limited	Wide	Wide	Wide
Complexity	Low	Moderate to High	Moderate to High	Moderate to High
Cost	Lower	Higher	Higher	Higher
Applications	Audio amplification	Power supplies	DC-DC converters	Power supplies

2.3 *Controllable Transceivers in Communication Systems*

With the increasing complexity and diversity of communication requirements, it has become essential to have flexible and adaptable transceivers in modern communication systems. In many applications, including wireless communication, Software-Defined Radio (SDR), and cognitive radio, being able to control and manipulate transceiver parameters in real time is crucial. Transceivers that support these applications require dynamic parameter adjustment to optimize performance, adapt to changing environments, and maintain a high level of compatibility.

Controllable transceivers are communication systems that can be controlled and modified programmatically. Several parameters can be adjusted in real-time, including frequency, bandwidth, modulation scheme, coding, and filtering. Controllable transceivers improve performance, flexibility, and compatibility by allowing the system to adapt to different communication scenarios.

The functionality of a controllable transceiver is achieved by combining several critical components in synergy. Universal Software Radio Peripheral (USRP)s, FPGAs, and microcontrollers are the three components that commonly make up controllable transceivers.

2.3.1 USRP

The USRP is a versatile and highly customizable hardware platform for RF applications. Users can create and deploy SDR systems using motherboards and daughterboards. FPGAs are integrated into the motherboard to facilitate real-time processing and communication with a host computer. A daughterboard, a radio front-end, houses the RF circuitry that transmits and receives signals. Several fields find extensive use for the USRP, including wireless communication research, spectrum monitoring, and radio system development. SDR solutions can be designed, prototyped, and implemented according to the application and requirements of users.

Figure 6: National Instruments USRP-2920 [44].

2.3.2 FPGA

FPGAs are integrated circuits that can be programmed after manufacture and configured [45]. The logic blocks are configurable, and the interconnects are programmable. In FPGAs, flexibility is a crucial characteristic, as users can configure the logic blocks and interconnections to build custom digital circuits and perform real-time processing. Among the many fields where FPGAs are used are digital signal processing, telecommunications, aerospace, and industrial automation. The advantages of these systems include their high computational power, parallel processing capabilities, and low-latency operations. In contrast to custom-designed Application-Specific Integrated Circuit (ASIC)s, FPGAs offer an advantageous platform for designing and prototyping complex digital systems.

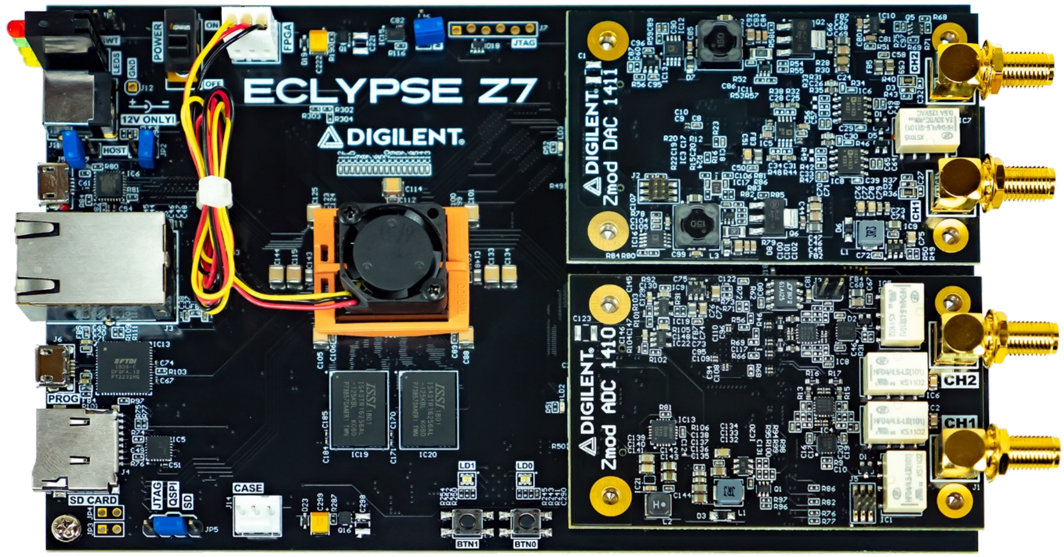

Figure 7: Eclypcse Z7 FPGA [46].

2.3.3 Microcontroller

An integrated microcontroller comprises a compact, standalone computer system on a single chip. The system includes microprocessors, memory, peripherals, and support components. With minimal external components, microcontrollers can perform dedicated tasks or control systems. It is commonly used in embedded systems for centralized intelligence and control of various devices and applications. Microcontrollers can be found in household appliances, automotive systems, consumer electronics, and industrial equipment. Many modern electronic systems provide the necessary computing power and functionality to perform specific tasks efficiently and reliably [47]. These are just a few examples, including Arduino, Raspberry Pi, STM32, and Peripheral Interface Controller (PIC). In addition to different manufacturers and models, microcontrollers are available in various features and applications.

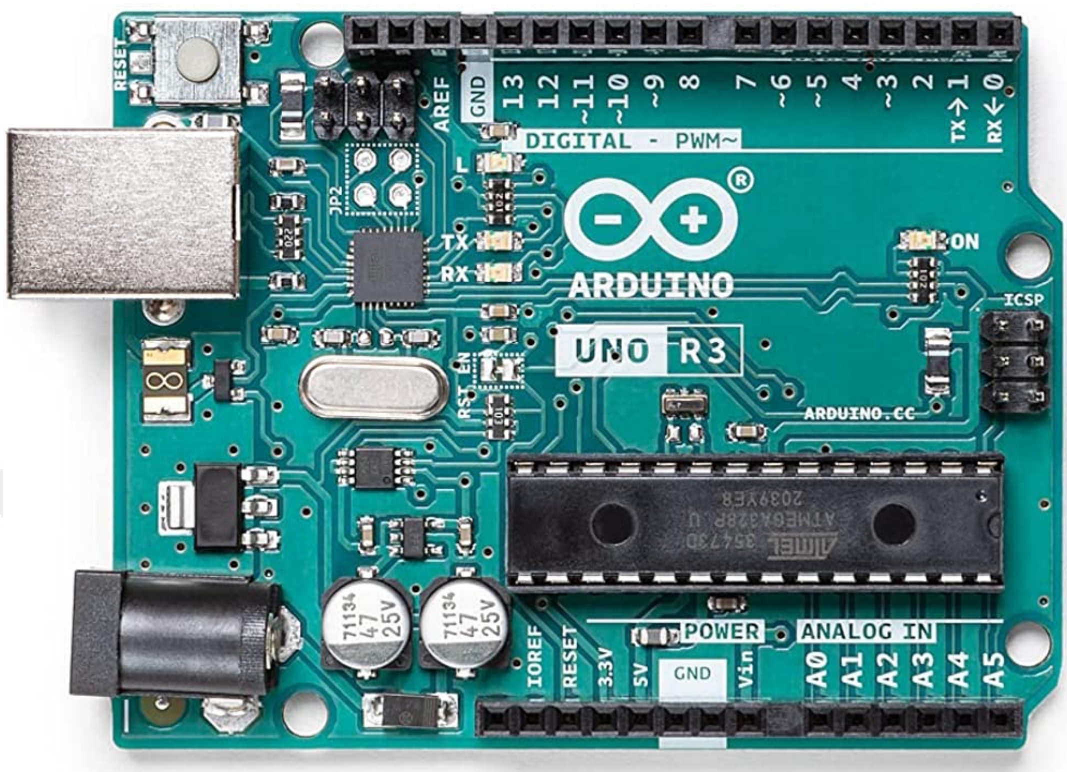

Figure 8: Arduino UNO microcontroller [48].

Each device category's specification limitations are highlighted in Table 4, including processing capabilities, Input/Output (I/O) options, and scalability. In addition, each device category is described in terms of the capabilities that make it suitable for a particular application. Its advantages include a wide frequency range, adaptability, flexibility, reconfigurability, and cost-effectiveness.

Table 4: Comparison of controllable transceivers.

	Advantages	**Limitations**
USRP	Wide frequency range. Large community and software. Software-defined radio capabilities.	Limited I/O options. Limited processing capability.
FPGA	High flexibility. High-speed parallel processing. Real-time performance.	Complex design. Requires specialized programming skills.
Microcontrollers	Quick development. Low power consumption. Ease of use.	Limited I/O options. Limited processing capability.

2.4 Photodetectors

In electromagnetic radiation detection, photodetectors are sensors that detect light [49]. A photodetector converts optical signals into electrical signals, and several applications rely on them to detect and measure light intensity. According to the photoelectric effect, photodetectors produce electrical signals when incident photons generate electron-hole pairs in photosensitive material.

2.4.1 PN and PIN Photodiodes

PN photodiodes are semiconductor devices with two terminals or electrodes. Diodes with one P-type side and one N-type side are called PN junction diodes. It is necessary to forward-bias the diode to allow current flow.

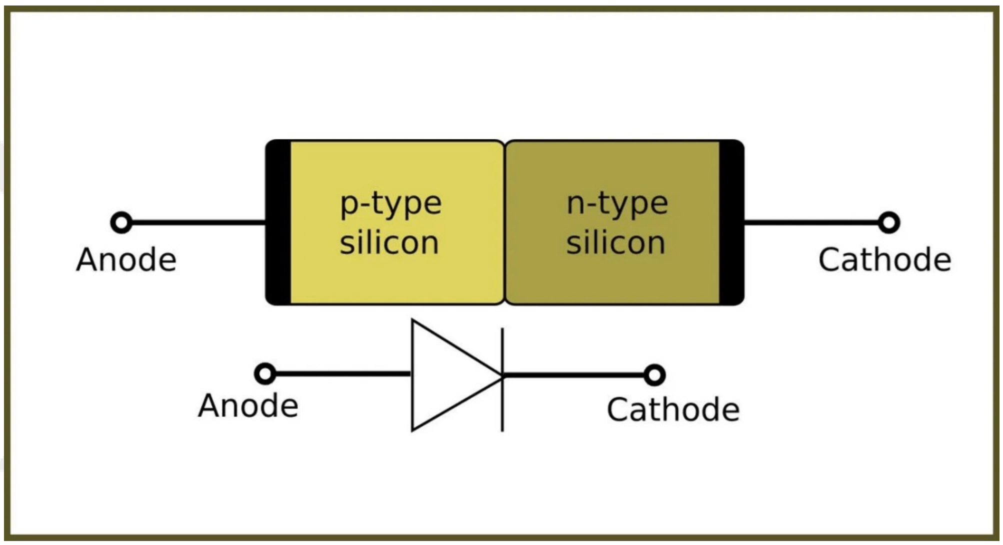

Figure 9: PN photodiode structure [50].

Connecting a positive voltage to the P terminal will cause current to flow from the P region to the N region. Current flow is blocked when the destruction zone on the P-type expands with negative voltage [50].

PIN-type photodiodes have an intrinsic layer (i.e., undoped) between the n-type and p-type dopings. Carriers generate the photocurrent in the intrinsic layer, where most photons are absorbed.

An anode is a ring-shaped electrode, whereas a cathode is a flat electrode. The bias voltage is reversed to connect the positive side to the negative side. P-doped regions are coated with anti-reflection coatings [50].

2.4.2 Phototransistor

A phototransistor is like a photodiode but has an additional amplification stage. Compared to photodiodes, they can provide a higher output current. Phototransistors are commonly used when low-light conditions or a higher sensing level are required. Their ability to amplify weak photocurrents generated by incident light leads to stronger electrical signals.

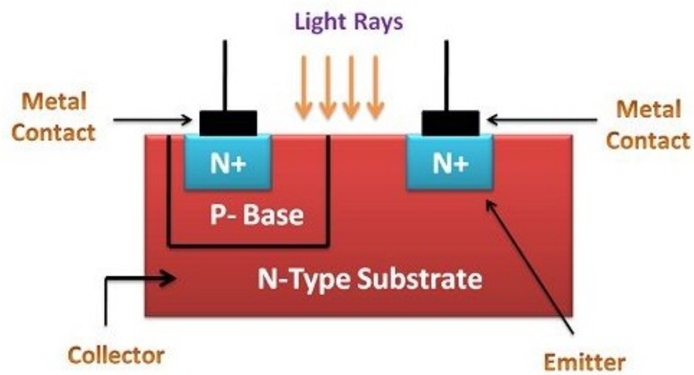

Figure 10: Phototransistor structure [51].

2.4.3 Photomultiplier Tubes

Photomultiplier Tube (PMT)s are susceptible devices used for measuring and detecting deficient levels of light. An electronic component, a photon converter, converts light particles into electrical signals. Photocathodes, dynodes, and anodes are all included in the PMT. Most photocathodes are composed of photosensitive materials such as cesium or gallium arsenide. In photocathodes, photons trigger the photoelectric effect, which emits electrons. The quantity of emitted electrons is indirectly proportional to the intensity of the incident light.

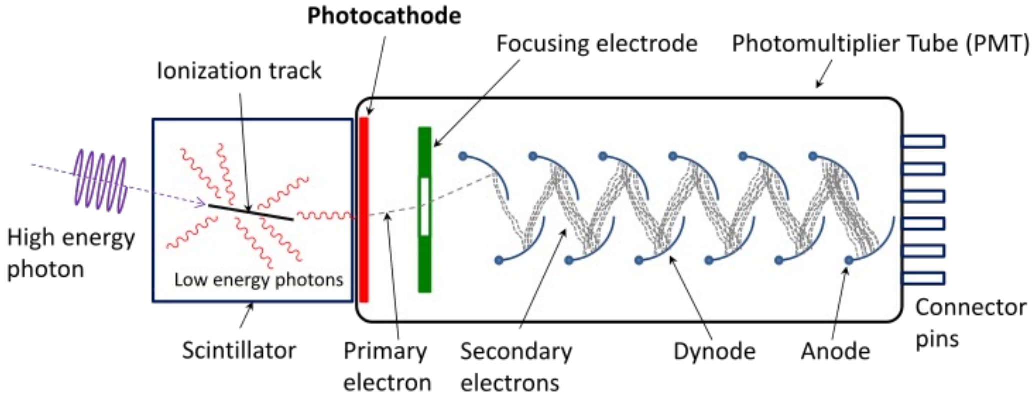

Figure 11: Photomultiplier tube structure [52].

Upon emitted electrons reaching the dynodes, they are accelerated towards a cascade of metal electrodes. Positive voltage is carried by each dynode slightly higher than the one before. In a process known as secondary emission, electrons collide with dynos and release additional electrons. The number of electrons exponentially increases as they pass from one dynode to the next during this multiplication process.

Ultimately, the electrons reach the anode, maintained at a high positive voltage. Anodes produce measurable currents and pulses that can be amplified and processed to produce output signals proportional to their intensity.

PMTs have several advantages, including remarkable sensitivity, rapid response time, a wide dynamic range, and minimal noise. These devices have numerous applications, including scientific research, medical imaging, particle physics, fluorescence detection, nuclear instrumentation, and astronomy, which require detecting feeble light signals.

2.4.4 Avalanche Photodiodes

The Avalanche Photodiode (APD) is another type that works as a photodiode but offers a high current gain because impact ionization occurs. A charge carrier with enough kinetic energy collides with another atom and dislodges electrons, resulting in impact ionization.

The avalanche effect is commonly known as this phenomenon. APDs are suitable for low-light conditions due to their sensitivity and current gain. Although it requires a high reverse voltage, it can introduce excessive electrical noise [53].

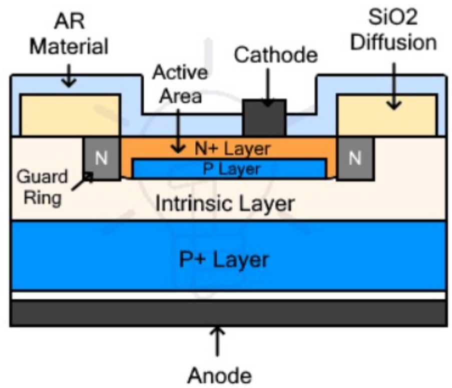

Figure 12: Avalanche Photodiode structure [53].

PIN photodiodes and APDs have similar structures. As illustrated in Figure 12, there are four layers. These are P, I, P, and N. During the electrochemical reaction, heavy doping of P+ and N+ acts as anode and cathode, respectively. Alternatively, there is an intrinsic I layer and a lightly doped P layer [53].

As APDs are highly sensitive, they can be used in various applications. These applications include photon counting, optical communication systems, and low-light imaging.

2.4.5 Charge-Coupled Device

In cameras, camcorders, and other devices that record pictures, CCD stands for Charge-Coupled Device. It converts incoming light into electrical signals to capture and process images. Unlike conventional sensors, Charge-Coupled Device (CCD) sensors are composed of tiny capacitors called pixels, which are sensitive to light. These pixels accumulate and store electrical charge depending on how much light they receive.

Capacitive coupling transfers the stored charge in each pixel sequentially or parallel to a shift register during image capture. Pixel by pixel, the shift register moves the charge across the sensor.

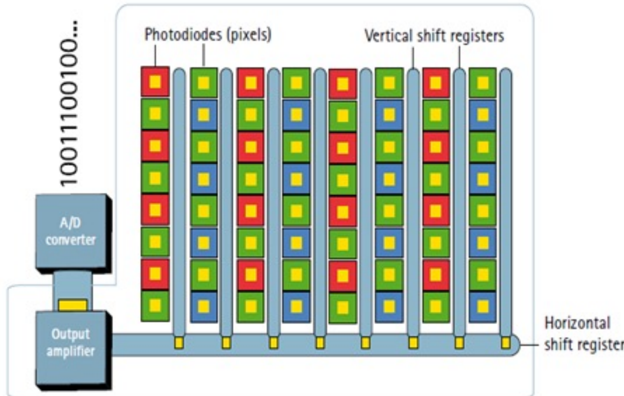

Figure 13: CCD sensor [54].

In order to process, store, or display the charge, it undergoes ADC conversion. It is then possible to manipulate, save, or transmit this digital representation of the image.

CCD sensors ' most notable properties are image quality, dynamic range, and noise performance. Their main strength is their ability to capture high-quality images in low-light conditions. The CCD sensors, however, usually consume more power and read out slower than CMOS sensors.

Scientific imaging, astronomy, and medical imaging have all found extensive applications for CCD technology.

2.4.6 CMOS Image Sensors

CMOS image sensors are used in digital cameras, smartphones, and other imaging devices for image capture and processing. CMOS image sensors consist of a grid of small light-sensitive pixels. The photodiode in each pixel transforms light particles (photons) into electric charges. A readout circuit embedded within the pixel receives this charge.

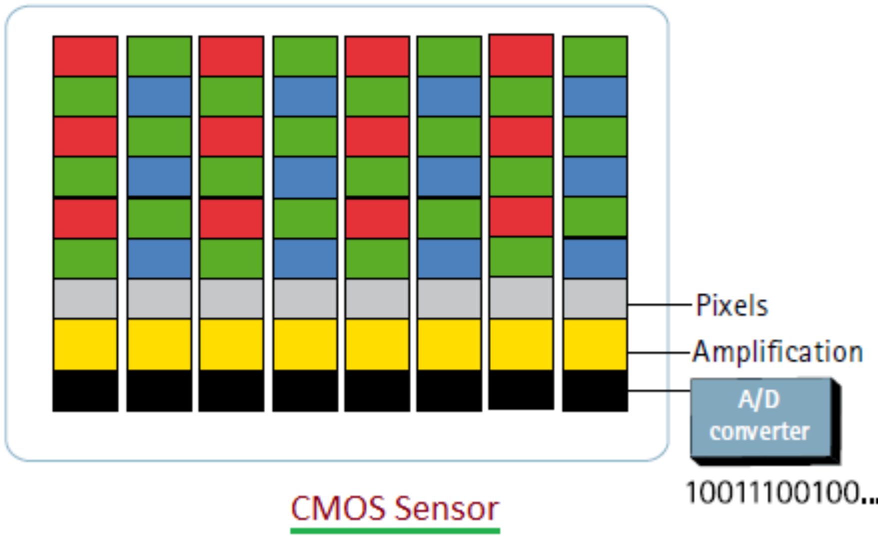

Figure 14: CMOS image sensor [54].

CMOS image sensors integrate signal amplification and processing circuitry directly into each pixel, unlike CCD sensors requiring additional amplification and conversion circuitry. By integrating these technologies, camera systems can be more compact and energy efficient.

The image sensor's detection of light exposes the pixels for a specific period. According to the sensor design, accumulated charges are read sequentially or parallel. Signals are amplified, converted into digital format, and then transferred for processing or storage by the readout circuitry.

In comparison to CCD sensors, CMOS image sensors offer several advantages. There are several advantages to this type of technology, including lower power consumption, faster readout speeds, and the ability to integrate additional features like on-chip image processing and pixel-level image correction. As a result of their versatility, cost-effectiveness, and performance advancements, they have become the dominant technology in consumer imaging devices.

Table 5 compares photodetectors, including PN diodes, PIN diodes, phototransistors, PMTs, APDs, CCDs, and CMOS sensors. The critical characteristics for communication purposes are highlighted in Table 5 which are responsiveness, speed, sensitivity, dark current, noise, and linearity.

Table 5: Comparison of photodetectors.

	Responsivity	Speed	Sensitivity	Dark Current	Noise	Linearity
PN	Moderate	Fast	Low-Moderate	Low	Low-Moderate	Moderate
PIN	Moderate	Fast	Low-Moderate	Low	Low-Moderate	Moderate
Phototransistor	Moderate to high	Moderate to fast	Moderate to high	Low to moderate	Moderate to high	Moderate
PMT	High	Moderate to fast	High	High	Moderate to high	Moderate to high
APD	High	Fast	High	Low-Moderate	Low-Moderate	Moderate
CCD	High	Moderate to fast	Moderate to high	Low	Moderate to high	High
CMOS	Moderate to high	Moderate to fast	Moderate to high	Low	Moderate to high	High

CHAPTER III

EXPERIMENTAL DEMONSTRATION

Two important steps are needed before the measurements that will be carried out in the next chapter. The first step was to make a decision on the equipment and hardware components which we did in the previous chapter. The second step is the system architecture, front-end design, and software which we discuss in this chapter. To make it clearer, in Chapter 2, we explored the hardware components frequently employed in streetlight VLC broadcasting. Subsequently, we compared these products within their respective categories. We identified the most suitable transmitter-receiver front-end components needed for our developed system.

In this chapter, we explain the system architecture we developed for experimental demonstration. Next, we explain the LED driver design, an essential part of the transmitter's front end. Following that, we introduce the system's receiver front end. Then we discuss implementation issues on FPGA the transmitter and receiver blocks.

Following is the remainder of this chapter. In Section 3.1 on the following page, we present the overall system architecture. In Section 3.2 on page 40, we design an LED driver for the transmitter's front end. In Section 3.3 on page 43, we present the receiver's front end. In Section 3.4 on page 44, we explain FPGA implementation for transmitter and receiver.

3.1 System Architecture

The block diagram of the overall system is provided in Figure 15.

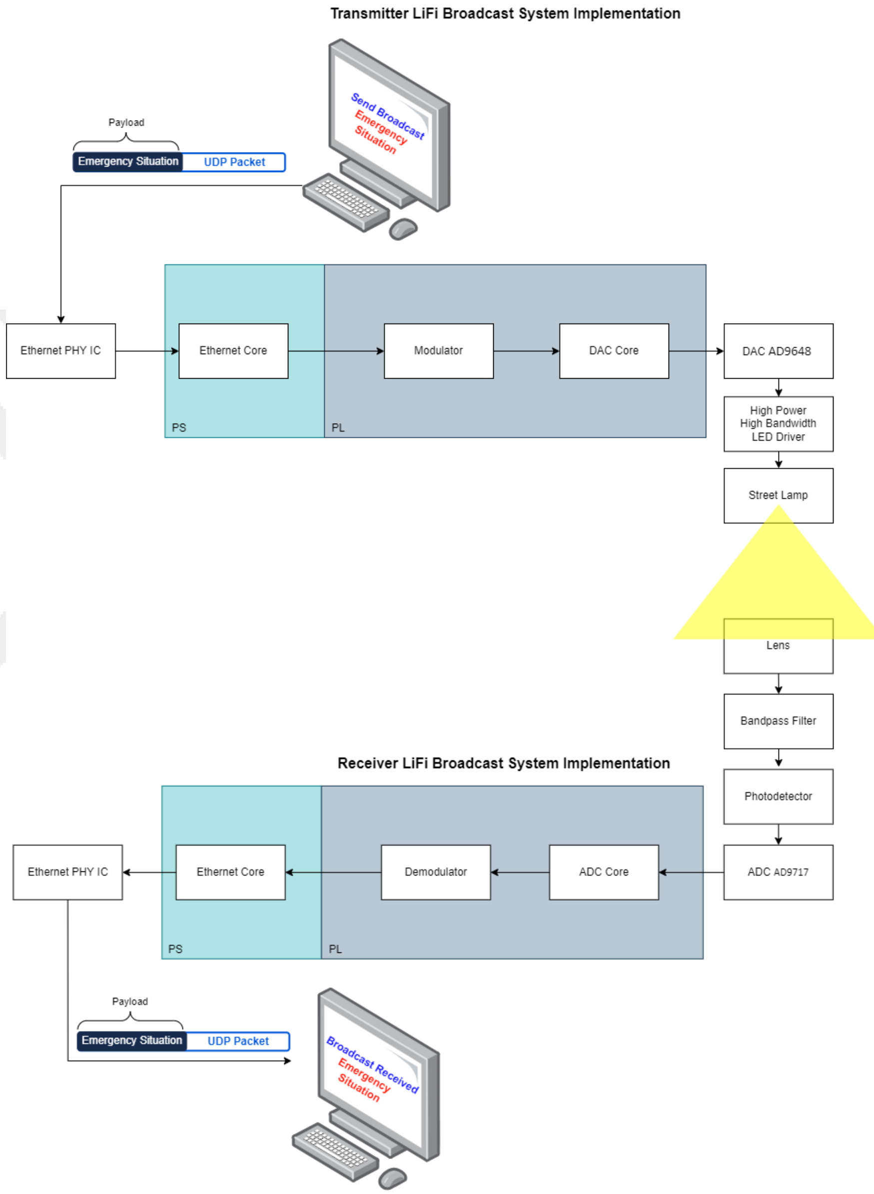

Figure 15: Overall system diagram.

For proof-of-concept system implementation, we will use Eclypse Z7 platform (see Figure 16.) which features ADC and DAC extension boards. The output of the DAC extension board has a sample rate of 100 Mega-Symbols Per Second (MS/s) while the ADC extension board has a sample rate of 125 MS/s. The sampling resolutions of both boards are 14 bits. The PS part of the FPGA design will have UDP server at the transmitter part where the packets will be fed from an external network. As soon as a packet arrives, it will transfer that packet to PL part of the FPGA through AXI bus between PL and PS parts. The PL will modulate the signal and feed the custom-design LED driver that drives an off-the-shelf streetlight. This driver will be designed for VLC such that it will have a large electrical bandwidth.

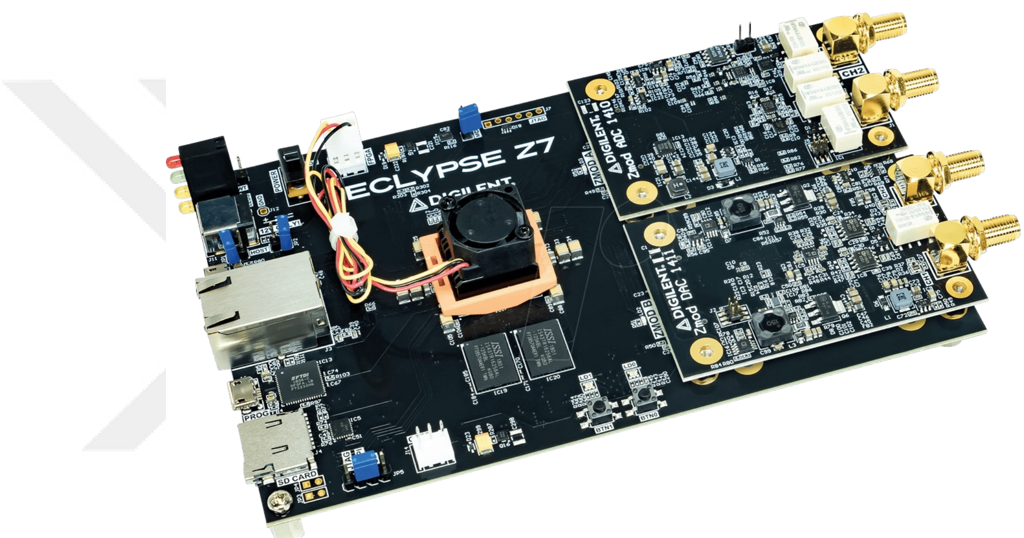

Figure 16: Eclypse Z7 FPGA Board with DAC/ADC extension boards [29].

After the transmitted signal goes through the propagation medium, it will be collected by a photodetector. A narrow-band optical filter will be used to prevent saturation and reduce environmental light noise. The analog output signal from the photodetector will be digitalized using ADC and fed to the demodulation block in the FPGA. Finally, the received package will be transferred to a previously defined IP address through Ethernet.

3.2 Transmitter Front-End

3.2.1 LED Driver Design

In our design, we selected an Efficient Power Conversion (EPC) 2052 Gallium Nitride (GaN) Power Transistor [55] (see Figure 17). The selected transistor has a high switching frequency effectively decreasing switching losses and reducing drive power. With a size of 1.5 mm x 1.5 mm, it has an ultra-small footprint.

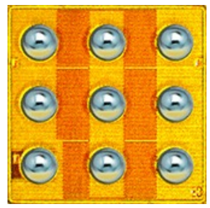

Figure 17: Used the transistor for LED driver (EPC 2052 GaN Transistor).

The input gates of GaN transistors are very sensitive. Instead of directly driving the transistor, we used Texas Instruments LMG1020 Low-Side GaN Driver [56]. This is a single, low-side driver designed for driving GaN Field-Effect Transistor (FET)s and logic-level MOSFETs in high-speed applications. Therefore, the modulation signal first goes to the GaN driver then fed to the base of the transistor. The schematic design is provided in Figure 18. Our driver design has 13.5 m ohm internal resistance and up to 72 Ampere driving capability.

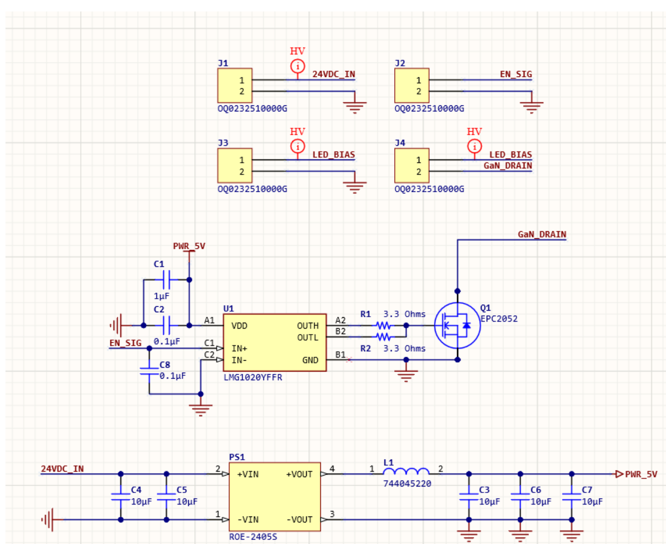

Figure 18: Schematic design of the high-power LED driver.

Figure 19 shows the Printed Circuit Board (PCB) design of a high-power LED driver.

The design has been made in 2 layers. The PCB material is Flame Retardant (FR) 4, and the thickness of the PCB is 1.6 mm.

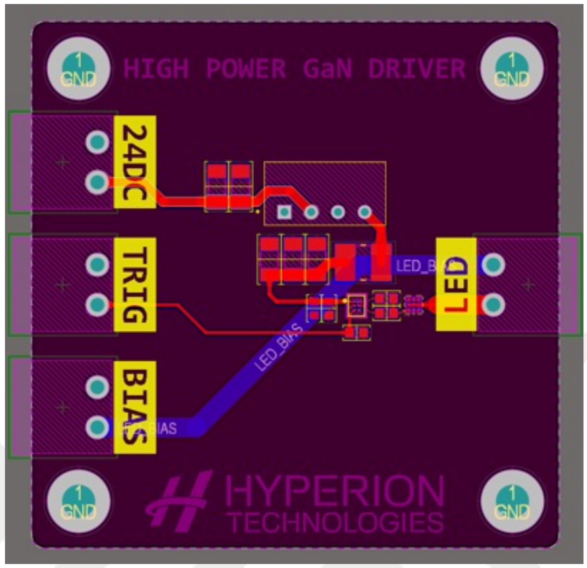

Figure 19: PCB design of high-power LED driver.

The picture of the manufactured LED driver is presented in Figure 20. We used a 24 V-to-5 V voltage regulator with filtering capacitors and inductors placed at the input and output of the system. The bias of LED is provided from a separate input, so we can test various LEDs without changing the LED driver circuit.

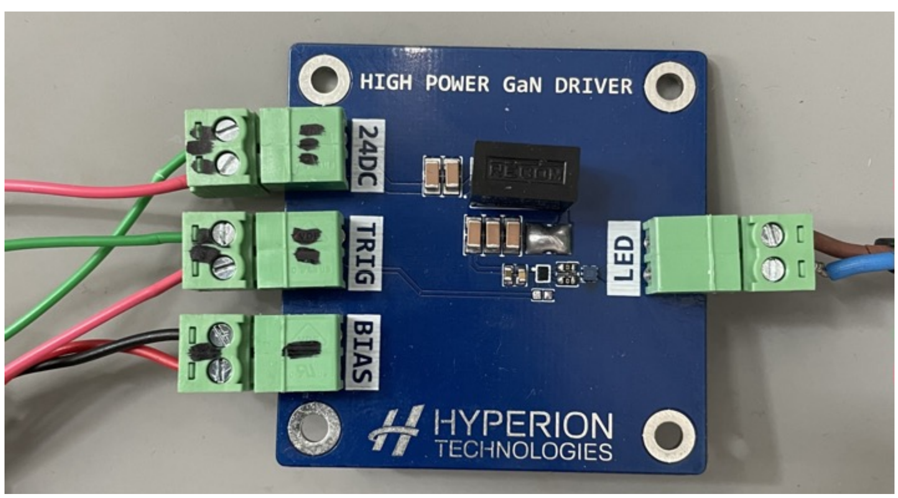

Figure 20: Manufactured and assembled high-power LED driver.

3.2.2 Streetlight

The PELSAN Madrid [57] streetlight, which offers economical pricing and a high efficacy factor, has been preferred for the experimental setup. PELSAN Madrid is used for various purposes, such as illuminating highways, squares, airports, gas stations, and parking lots. It features 36 Samsung LM302Z LED chips.

Figure 21: PELSAN Madrid streetlight.

3.3 Receiver Front-End

In the Thorlabs APD130A/M [58] series, avalanche photodetectors are combined with a specially designed trans-impedance amplifier with ultra-low noise and temperature compensation. This detector can detect a DC to 50 MHz optical signal. This light series is well suited for applications such as spectroscopy, fluorescence measurements, laser radar, and optical rangefinders due to their extremely low Noise Equivalent Power (NEP). In many applications, they can replace PMTs due to their high sensitivity. PMTs are susceptible to unwanted ambient light, but APDs are not. At the receiver front end, an APD collects an optical signal and produces a photocurrent. The output analog signal from the photodetector is read by the ADC and transmitted digitally to the FPGA.

Figure 22: Thorlabs APD 130A/M [58].

3.4 FPGA Implementation

The system is built upon the Eclypse Z7 FPGA platform. It is implemented using C and VHDL languages on the Eclipse Z7 platform, which has a Xilinx Zynq-7010 System-on-Chip (SoC) FPGA. C programming language is used on the PS side, and VHDL programming language is used on the PL side. The PL part of the FPGA typically handles signal modulation and demodulation, which are time-critical and processing-intensive steps. The PS part provides packet forwarding and Ethernet communication of the VLC system with external networks. UDP packets are created with Python software on the transmitter laptop and are transferred to the transmitter FPGA via an Ethernet cable.

3.4.1 Frame Structure

The frame structure is illustrated in Figure 23. Each frame has a header, a length of information, and a footer. Frame detection is based on the header and footer. At the receiver side, the photodetector output is transferred to the FPGA. The FPGA first demodulates the first bit of the header. When it demodulates the first bit correctly, it demodulates the second and third bits. When the demodulator correctly decodes the first three bits, it decodes the entire payload until the footer arrives. When the entire payload is demodulated, PS transfers the payload to the receiver laptop via an Ethernet cable.

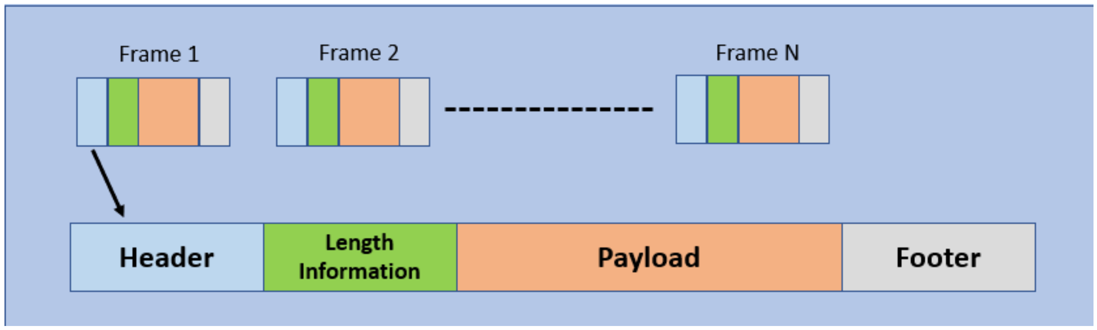

Figure 23: Frame structure.

3.4.2 Transmitter FPGA Implementation

Figure 24 shows the inner blocks of the Eclypse Z7 Board. The Zynq All Programmable System-on-Chip (APSoC) on the board includes two distinct subsystems. These are the PS and the PL. As the input, we create UDP data with Python and send it to Eclypse Board via Ethernet.

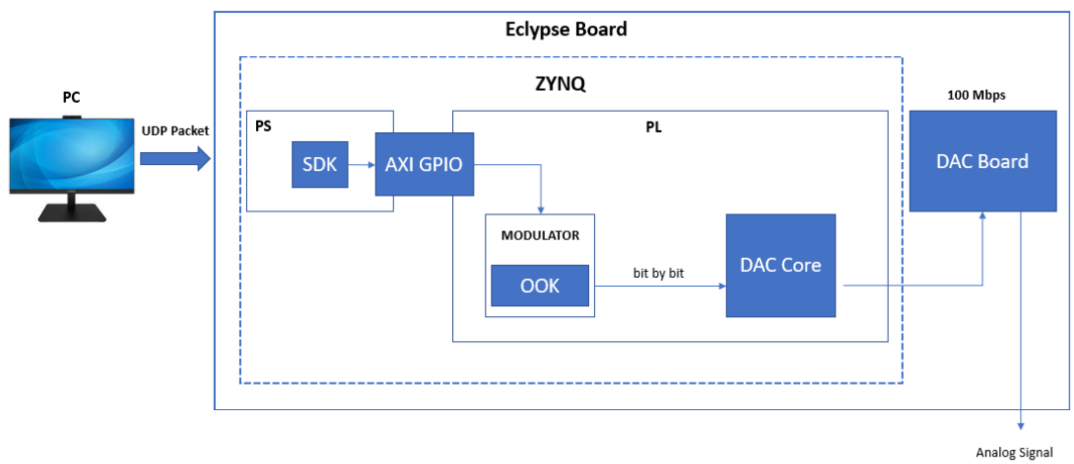

Figure 24: Inner blocks of Eclypse Z7 board.

Figure 25 shows the inner blocks of the PS and PS-Ethernet core. The Eclypse Z7 uses a Realtek RTL8211E-VL PHY to implement a 10/100/1000 Mb/s Ethernet port for the network connection between the RJ45 socket and the FPGA. The RTL8211E-VL PHY supports Reduced Gigabit Media Independent Interface (RGMII) communication. The Management Data Input/Output (MDIO) connects the RTL8211E-VL PHY and Ethernet Media Access Control (MAC). The Management Data Clock (MDC) is the bus clock provided by the MDIO. The Software Development Kit (SDK) is the Integrated Design Environment (IDE) for creating embedded applications on Zynq APSoC. The implementation of the SDK is done using C language. The AXI General Purpose Input/Output (GPIO) core provides a general-purpose input/output interface between PS and PL. SDK buffers incoming UDP packets to PL through AXI GPIO.

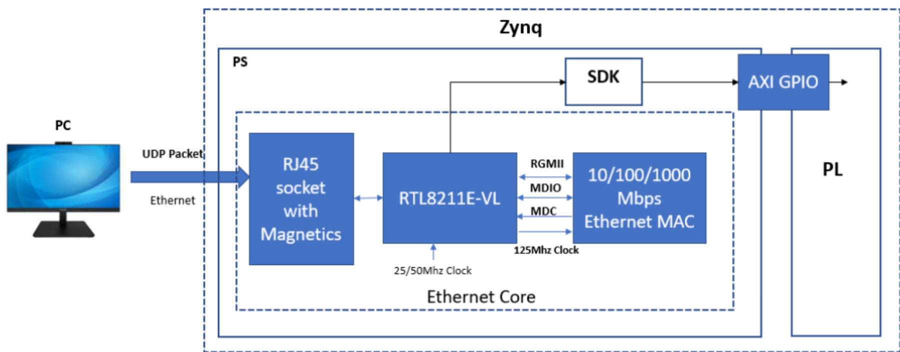

Figure 25: Inner structure of PS-Ethernet core.

Figure 26 shows the inner blocks of the PL. The AXI GPIO uses the Xil_Out32 command and writes UDP packets to Block Random Access Memory (BRAM). The AXI GPIO uses BRAM to transmit UDP packets to the PL part. The Xil_Out32 command writes data to BRAM each with a length of 32-bit. The data also includes the length information.

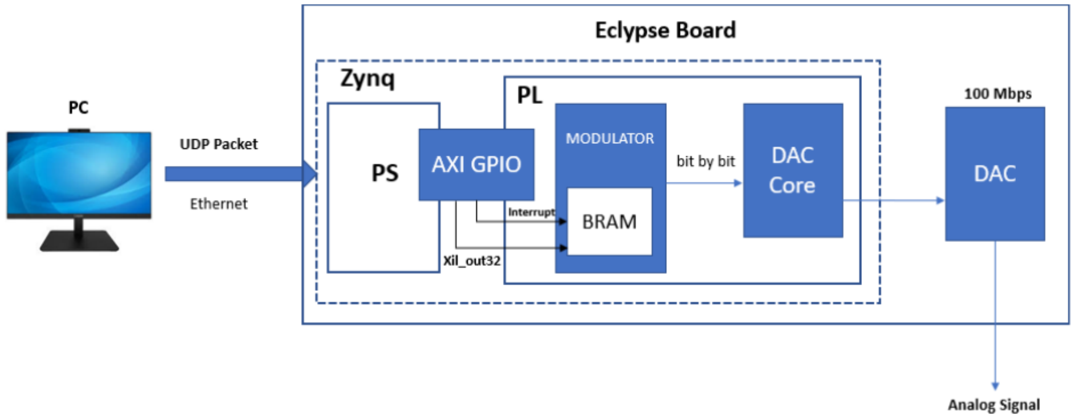

Figure 26: Inner structure of PL.

Figure 27 shows the state machine associated with the modulator. The PS writes UDP packets to BRAM at the address 0x40000000. After writing UDP packets to BRAM, the AXI GPIO sends an interrupt signal from the PS to PL. The PL detects the signal, and the modulator starts the *memory_tx* block. The state machine consists of two processes as detailed below.

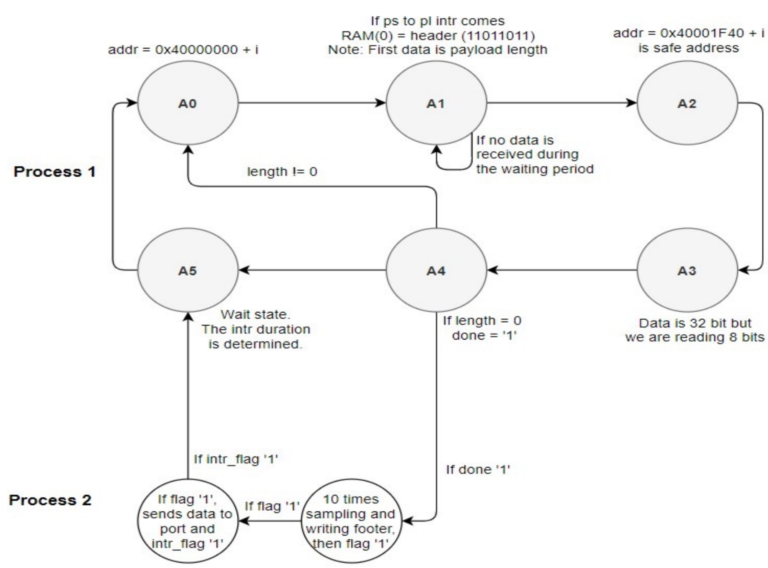

Figure 27: State Machine Diagram.

- **Process 1:** Initially, the address is set as 0x4000000 in state $A0$. With the incoming input data, the system goes into state $A1$. The system stays in the $A1$ state until the interrupt signal comes from PS to PL, then the system starts reading from address $0x40000000$ at the BRAM. The first read data is length, which is saved as a temporary variable. The 8-bit data is added to the first slot of the 8-bit array called Random Access Memory (RAM), and the system enters the $A2$ state. In the $A2$ state, the BRAM address is set to the safe address value and the system enters the $A3$ state. In the state $A3$, if the secure address value is in the initial state $0x4001F40$, the payload length information writes to the second and third slots of the RAM array element, otherwise, the least significant 8 bits of the received data are overwritten to the RAM array element. The received data is also saved to the secure address and the system switches to the $A4$ state. The $A4$ state checks if all data has been read from BRAM, in which case it writes 8-bit footer data to the last slot of the RAM array element and generates a $'done'$ signal. This moves the system to the standby state $A5$, otherwise, the BRAM read cycle returns all data to BRAM. The system comes to the $A0$ state and repeats until all the data is read.

- **Process 2:** If all the data is read from BRAM, it samples 10 times per 8-bits of data and sent bit-by-bit to the DAC in the module. When all data is sent, it generates an interrupt flag that removes the $A5$ state from standby and a PL to PS interrupt signal is sent to notify the PS that the Transmitter (TX) data is being sent to the DAC for transmission.

Figure 28 shows the processing of the DAC Core. The input of this block is 1-bit, and the output is 14-bits. For the DAC input, it converts from 1 to 8100 (decimal) and 0 to 100 (decimal), so it gets a square wave with high-level 8100 and low-level 100. These signals are fed to the DAC.

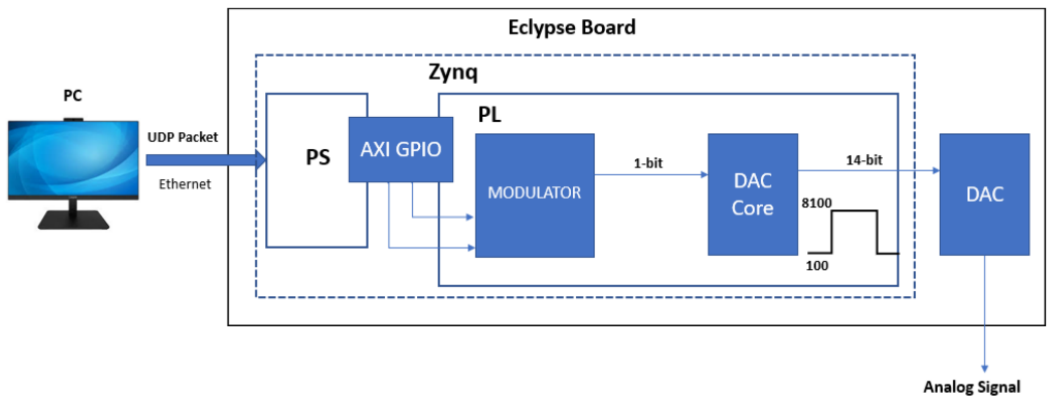

Figure 28: DAC core.

3.4.3 Receiver FPGA Implementation

At the receiver side, we have a front-end (including a photodetector and a transimpedance amplifier) that interfaces with the FPGA. The output of the receiver front-end is an analog signal which will be fed to the ADC with an SubMiniature version A (SMA) cable.

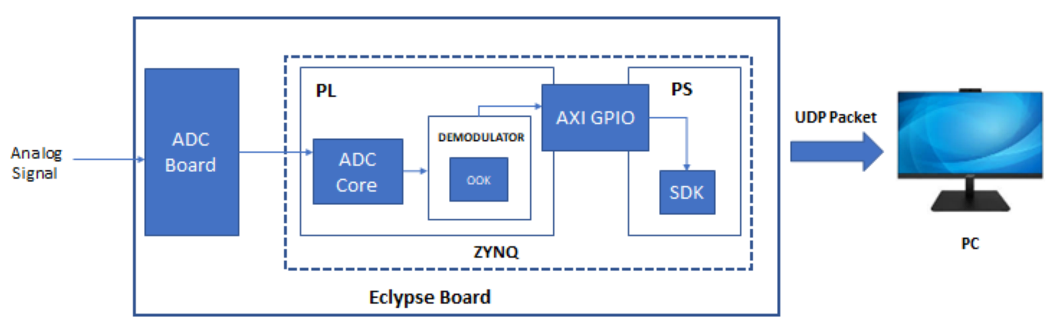

Figure 29: Receiver blocks.

Figure 30 shows the inner blocks of the PL sub-system. The signal from the ADC enters the ADC Core as 16 bits. ADC Core transfers 16 bits to the *Data Shift Block*. Shift operations are accomplished with multiplication and division by powers of two. Shifting the bits to the left does the multiplication, and shifting the bits to the right does the division. The *Data Shift Block* decreases the amplitude of the incoming signal. The analog signal amplitude is reduced by 4 times to make the calculations in the *Threshold Block* easier.

This module clears 2 bits by shifting the data 2 bits to the right. The output of this block is still 16 bits.

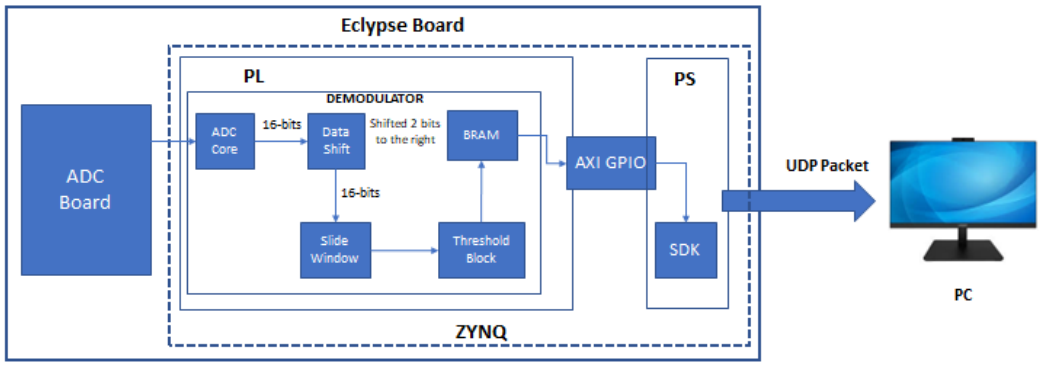

Figure 30: Inner blocks of the PL sub-system.

The *Sliding Window* block sends each received 16-bit data to 10 shift registers. The outputs of each register are then summed. As a result of this sum, the output of this module turns into a triangle, the highest value being $8100x10$ and the minimum being $100x10$. The threshold value for the detection of 1s and 0s is then determined by the *Threshold Block*.

Figure 31 shows the State Machine (SM) associated with the *Threshold Block*. The *Threshold Block* waits to receive the header byte, after which it locks itself until the successful reception of the complete payload. After the footer is decoded, the *Threshold Block* returns to its initial state and waits to receive the header of the next payload.

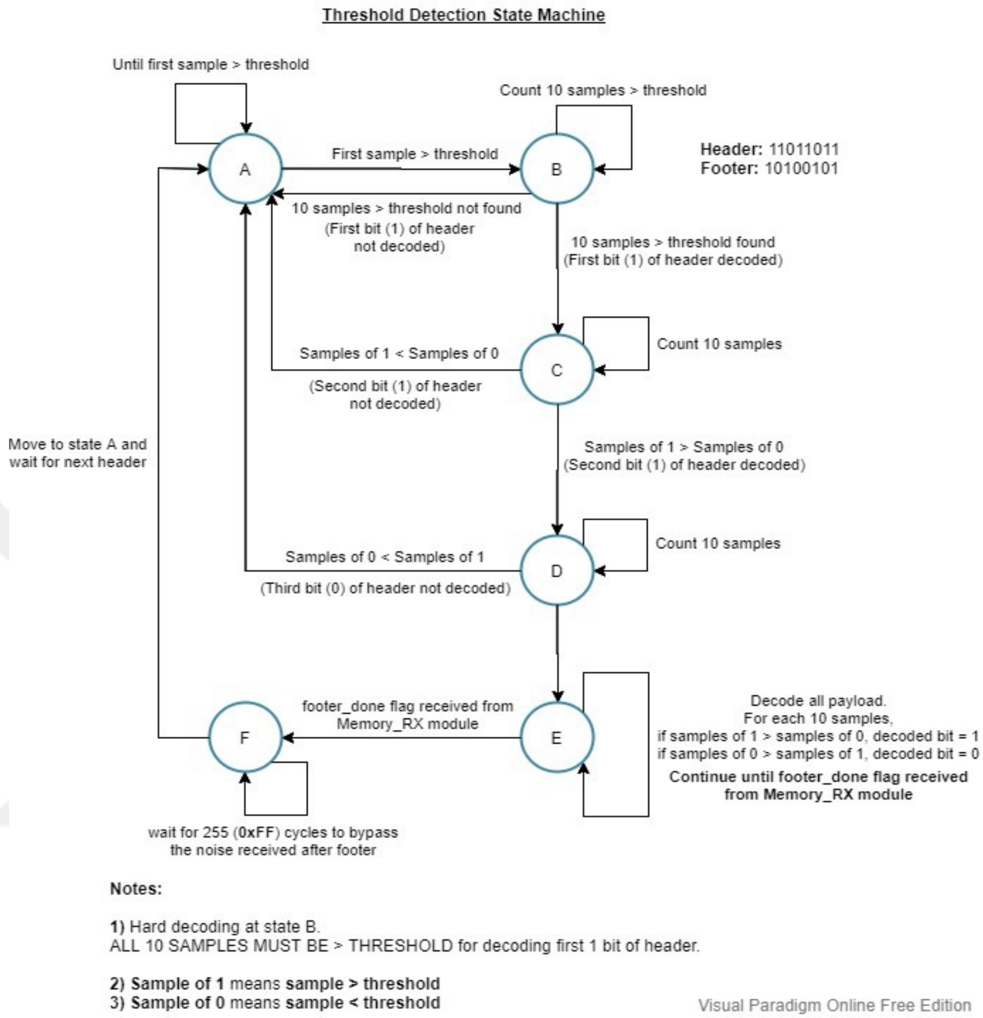

Figure 31: State Machine diagram of Threshold Block.

The header is given by [1 1 0 1 1 0 1 1]. The *Threshold Block* determines the first bit in the header as the first step. In state A, the *Threshold Block* waits for the first sample larger than the threshold. Once this is found, SM moves to state B.

In state B, the SM continues to count the remaining samples of the first bit of the header. If all 10 samples larger than the threshold are received, the first bit of the header is successfully decoded, and the SM moves to state C. If less than 10 samples larger than the threshold are received, the SM moves back to state A. This hard decoding logic of having all 10 samples larger than the threshold and no tolerance of having any sample smaller than the threshold is employed in state *B*. Because the first two bits of the header are both 1, which indicates the arrival of a valid header, then the first 10 samples will be greater than the threshold. So, no tolerance is allowed for samples smaller than the threshold in state *B*.

In state *C*, the SM counts 10 samples again. If the number of samples larger than the threshold exceeds the number of samples smaller than the threshold, the second bit of the header is also successfully decoded, and the SM moves to state *D*. Otherwise, the SM moves back to state *A*.

In state *D*, the SM counts 10 samples again. If the number of samples smaller than the threshold exceeds the number of samples larger than the threshold, the third bit of the header is also successfully decoded, and the SM moves to state *E*. Otherwise, the SM moves back to state *A*.

States *B*-*D* bring robustness in the detection of header. After the first three bits [1 1 0] of the header are successfully decoded by states $B-D$, state *E* begins decoding the entire payload till the arrival of the footer. The footer is in the form of [1 0 1 0 0 1 0 1]. The logic is the same as in states *C* and *D*. The state counts 10 samples. After every 10 samples, if the number of samples larger than the threshold exceeds the number of samples smaller than the threshold, the bit is decoded as 1; otherwise, it is decoded as 0. The BRAM block appends these decoded bits and converts them to bytes. After the footer byte is received, BRAM sends a $footer\_done$ flag to the $Threshold\ Block$. Then SM moves to state F. The footer bits are followed by some noisy 1s and 0s before settling to a steady state of 0. Therefore, a wait state F is added before returning to state *A*. This state waits for 255 $(0xFF)$ cycles before returning to state *A*.

Figure 32 shows the input of the $Threshold\ Block$ using Integrated Logic Analyzer (ILA) dumps. Based on this plot, to ensure that both 1s and 0s have the best chance of having 10 samples each, the threshold value is set as 123590 (decimal) = 00011110001011000110 (binary).

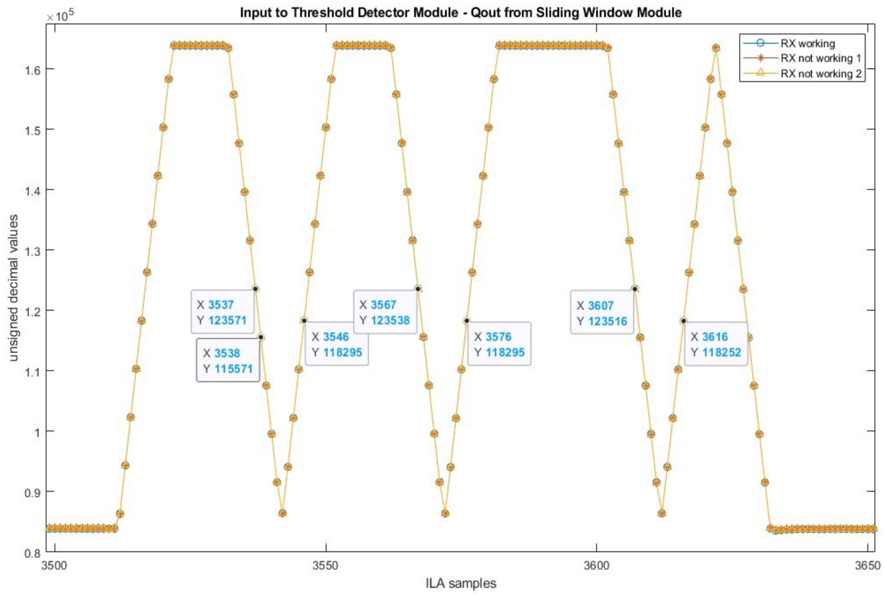

Figure 32: Input of threshold block.

Figure 33 shows the SM of the BRAM block. This block consists of two SMs. The first SM (states $A0$-$A4$) adds the bits received from the *Threshold Block* to the bytes. Then, it saves them in temporary memory until the footer bytes are received. Then it creates a flag to start the following SM (states $B0$-$B4$). This SM writes the data saved in the temporary memory to BRAM for subsequent reading by the PS side.

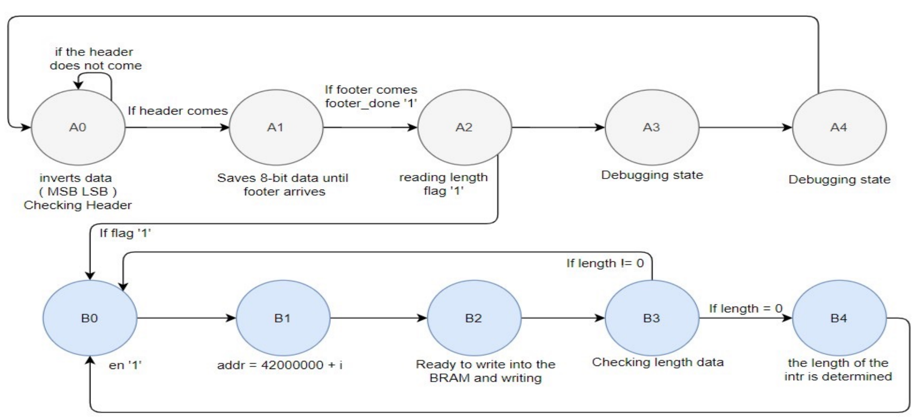

Figure 33: State Machine diagram of BRAM.

Figure 34 shows the inner blocks of the PS and PS-Ethernet core. The Eclypse Z7 uses a Realtek RTL8211E-VL PHY to implement a 10/100/1000 Mb/s Ethernet port for the network connection between the RJ45 socket and the FPGA. The RTL8211E-VL PHY supports RGMII communication. The MDIO connects the RTL8211E-VL PHY and Ethernet MAC. The MDC is the bus clock provided by the MDIO. The SDK is the IDE for creating embedded applications on Zynq APSoC. The AXI GPIO core provides a general-purpose input/output interface between PS and PL. SDK buffers incoming UDP packets to RTL8211E-VL throughAXI GPIO. As the output, UDP sends data to the Receiver (RX) PC via Ethernet.

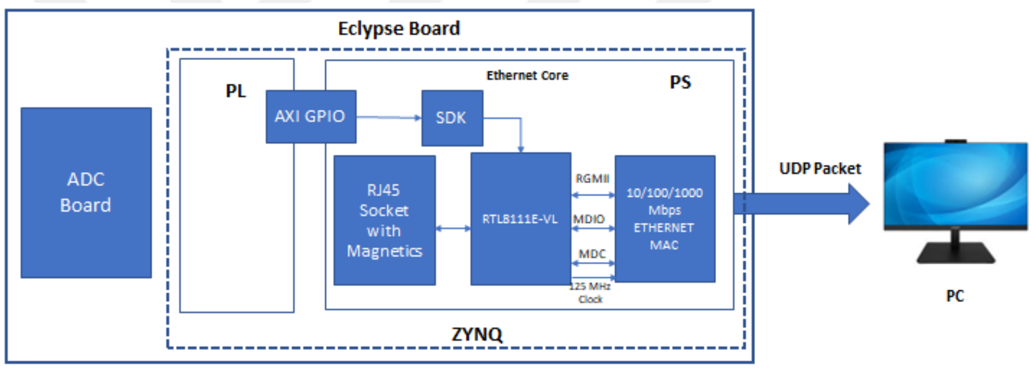

Figure 34: Inner structure of PS-Ethernet core at the receiver side.

CHAPTER IV

MEASUREMENT CAMPAIGNS AND RESULTS

In the preceding chapters, we did all of the needed steps for experimental results, which included deciding on the hardware component (See Chapter 2) and system architecture in addition to the software implementation (For more details, please see Chapter 3). In this chapter, we discuss photometric quantities for streetlights. Next, we provide our performance measurement campaigns and results.

Following is the remainder of this chapter. In Section 4.1, we discuss photometric quantities for streetlights, and we measure the streetlight that is used for experimental demonstration. In Section 4.2 on page 58, we present the bandwidth for our streetlight. In Section 4.3 on page 59, we present BER performance and the impact of the matched filter in experiments conducted in the indoor environment. In Section 4.4 on page 68, we present SNR performance while BER is zero conducted in the outdoor environment.

4.1 Photometric Quantities

Goniophotometers measure a light source's photometric properties or light distribution pattern. Light sources, such as lamps, luminaires, LEDs, and other lighting devices, are commonly assessed using this test in lighting design, research, and quality control.

The goniophotometer measures light distributions in different directions emitted by a source. Detailed information about light intensity, color, and angular distribution is provided, allowing a comprehensive evaluation of the light source's performance. An angle-dependent goniophotometer can produce a photometric diagram or polar plot with the data collected at specific angles.

A goniophotometer measures light sources or luminaires by rotating or tilting a platform. A highly sensitive photodetector measures the light output at various angles as the sample is rotated or tilted. The goniophotometer can capture an angular variation in light intensity in this way, enabling it to create a complete photometric profile.

As shown in Figure 35, there are 3 types of goniophotometers. These are Type *A*, Type *B*, and Type *C*.

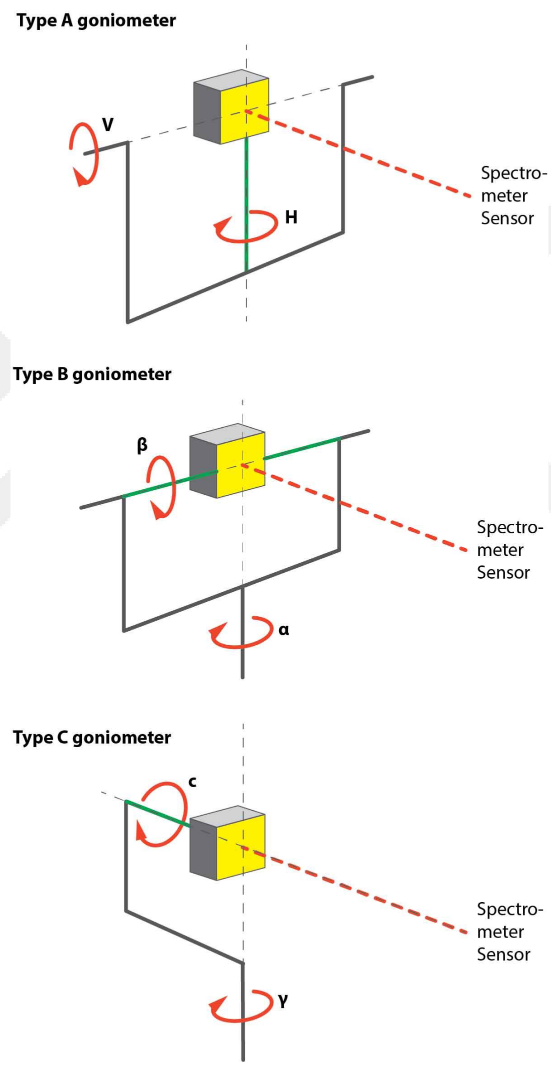

Figure 35: Goniophotometers types [59].

4.1.1 LabSpion Goniophotometer

Whether outdoor luminaries, automotive headlights and taillights, or LED luminaries, the LabSpion goniophotometer is ideal for measuring a wide range of light sources. In addition to being easy to attach to the goniophotometer, rotation is also quick and quiet. The LabSpion can handle light sources weighing up to 25 kg and having a diameter of 1.5 m. Light sources weighing 45 kg and measuring 2.0 meters can be handled with the heavy-duty 2.0 m tower version [60]. The LabSpion goniophotometer is a Type *C* goniophotometer. A spectrometer sensor gives the measurement results to the user thanks to its software.

Figure 36: LabSpion Goniophotometer [60].

4.1.2 Measurement Results

A PELSAN Madrid streetlight was connected to the LabSpion goniophotometer, and the measurement was taken. The measurement results are shown in Table 6.

Table 6: Photometric values for PELSAN Madrid streetlight.

	Luminous Flux (Lumen (lm))	**Luminous Intensity (Candela (cd))**	**CRI**	**Color Temperature (Kelvin (K))**	**Power (W)**	**Light Efficiency (lm/W)**
PELSAN Madrid	2731	1520	83,6	4009	20	141

Figure 37 shows the radiation pattern of the PELSAN Madrid streetlight. It consists of 36 LED chips. Each chip radiates 0.54 W with a full angle of half power of 110.4°. It has an asymmetric beam structure as a radiation pattern classification.

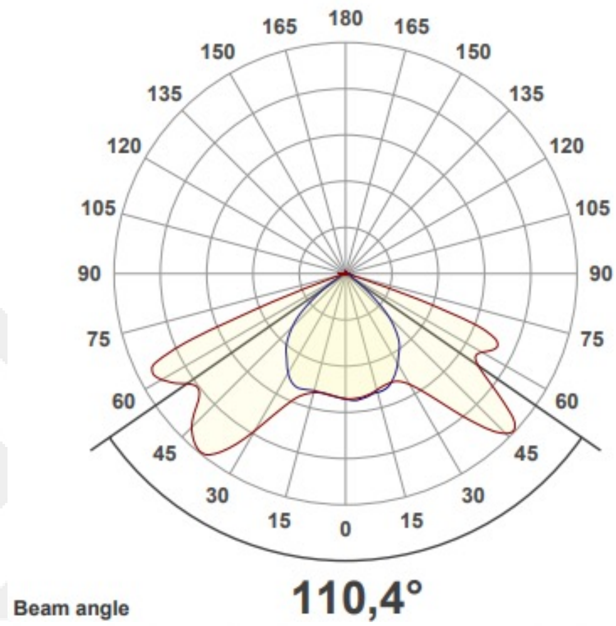

Figure 37: The radiation pattern of PELSAN Madrid streetlight.

The primary purpose of goniophotometer measurements is to obtain the necessary data for calculating BER and SNR, such as transmit power and radiation pattern, etc., and to confirm the datasheet of the streetlight.

4.2 Bandwidth

Bandwidth refers to the measurement of a signal's or transmission's bandwidth. Bandwidth describes the range of frequencies that can be transmitted or processed by a device or system in electronics and communication.

We measured the bandwidth of the streetlight. For this purpose, we generated a wide frequency range signal from the signal generator and analyzed the resulting signal with APD in the spectrum analyzer.

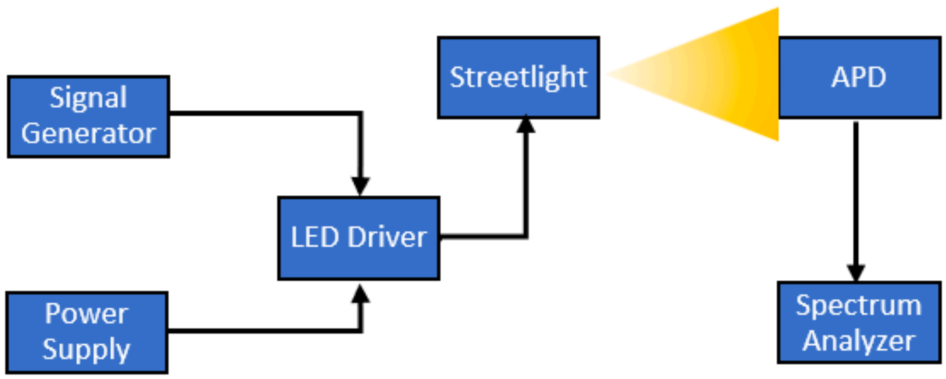

Figure 38: Block diagram of the experimental setup.

The 3 dB bandwidth of the streetlight was measured as 495 kHz in Figure 39, which should be sufficient for broadcasting messages in public safety applications.

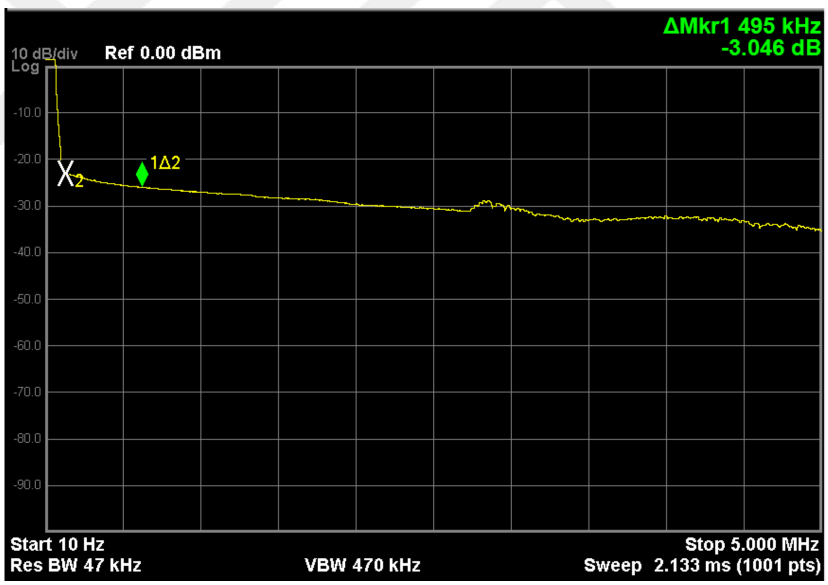

Figure 39: The 3 dB bandwidth of the PELSAN Madrid streetlight.

4.3 Indoor Scenarios

In this section, we will discuss scenarios conducted in the laboratory environment. We will examine the system's distance-dependent BER performance without performing a matched filter. In the other scenario, we will compare the system's distance-dependent BER vs SNR performance with theoretical values by applying a matched filter.

4.3.1 Without Matched Filter Bit Error Rate Measurements

Figure 40 illustrates the end-to-end block diagram of our experimental setup. The laptop with Python software generates the digital signal as the UDP packets at the transmitter side. Then, these UDP packets are transferred to the Eclypse Z7 FPGA with Zmod 1411 daughterboard through an ethernet cable. The transmitter front-end includes a high-power LED driver and an off-the-shelf streetlight. At the receiver front-end, Thorlabs APD130A/M collects an optical signal and produces a photocurrent. The output analog signal from the photodetector is read by the ADC and transmitted digitally to the FPGA. Figure 41 illustrates the experimental setup during measurements.

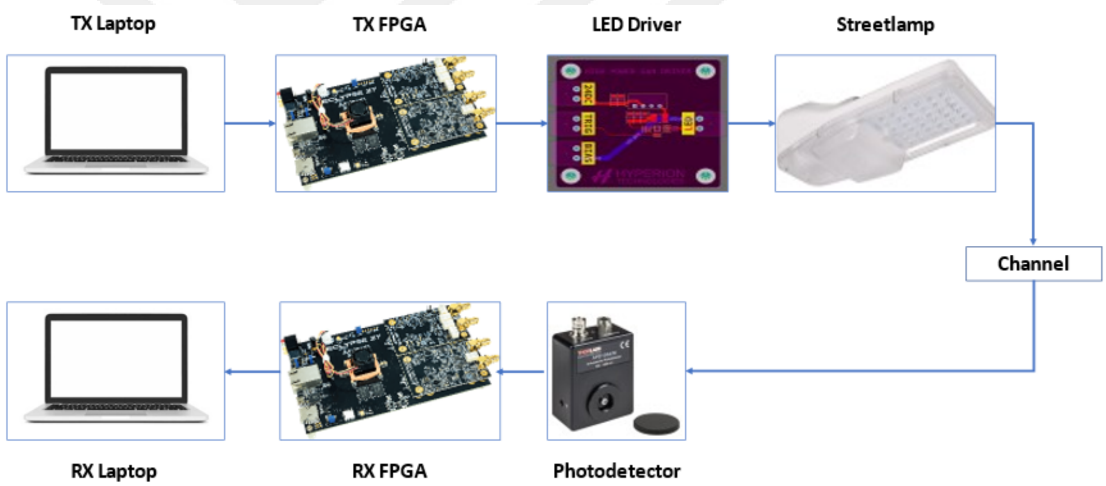

Figure 40: Block diagram of the experimental setup.

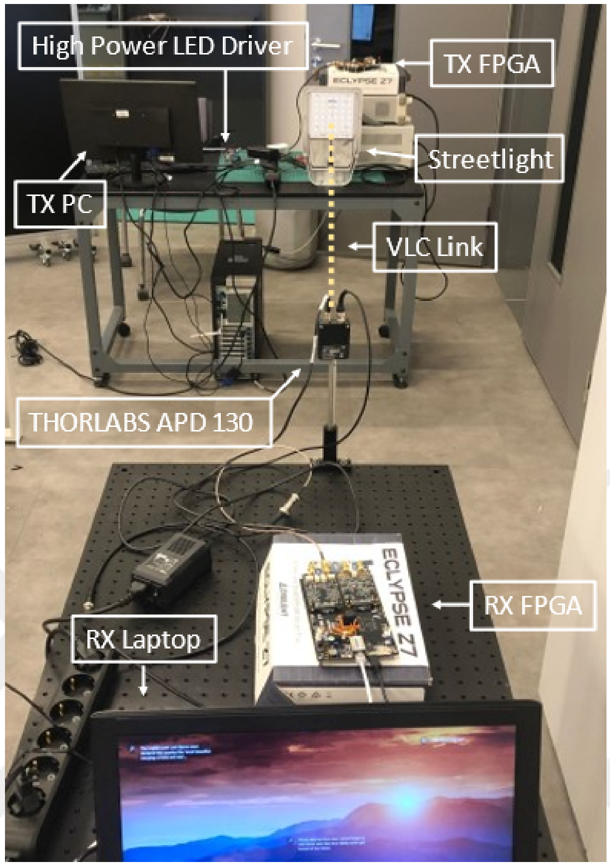

Figure 41: Experimental setup during measurements.

LOS and Non-Line of Sight (NLOS) scenarios were considered. In the LOS scenario, the transmitter and receiver are in perfect alignment. In the NLOS scenario, the receiver front-end is positioned 1 m above the situation in the front-end LOS scenario. Figures 42 and 43 show LOS and NLOS scenarios, respectively.

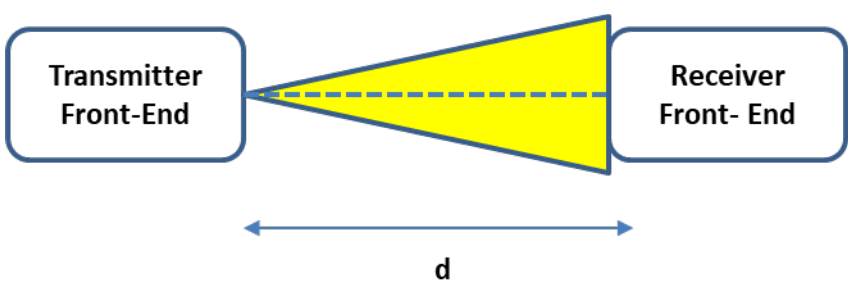

Figure 42: LOS scenario.

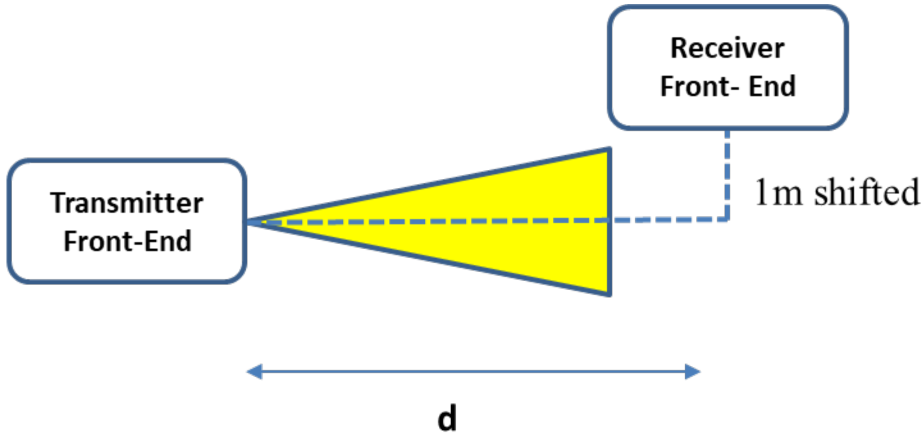

Figure 43: NLOS scenario.

In Figure 44, we present the error rate performance of our VLC system set-up. The experiments are conducted for distances from d = 0.5 m up to d = 9 m with 0.5 m intervals. For each point, the transmitted frames were collected through the Wireshark software, and the error rate was computed from the received frames afterward.

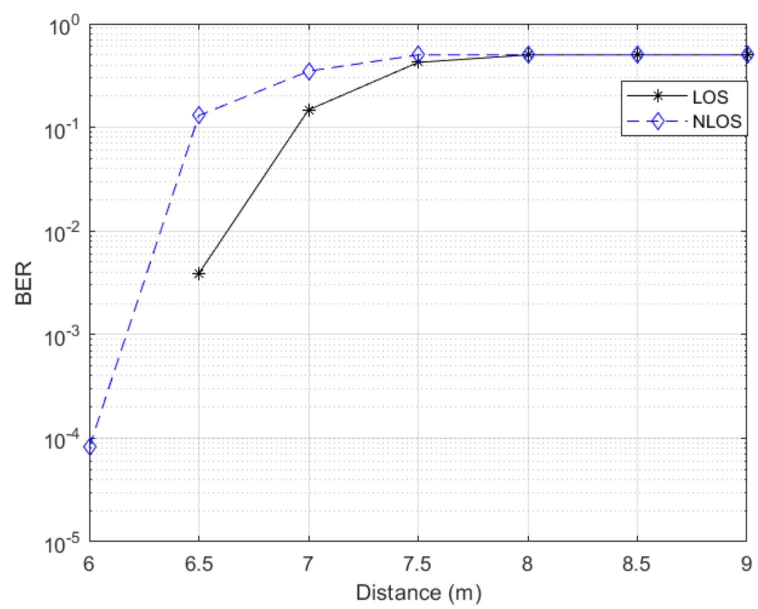

Figure 44: Bit error rate results.

In the first test scenario where there is perfect alignment between transmitter and receiver, errors were first observed at $d = 6.5$ m, and a BER of $P_e = 3.8 \times 10^{-3}$ was recorded. Shifting the receiver front end by 1 m resulted in a worse BER performance of $P_e = 1.3 \times 10^{-1}$ at the same propagation distance of 6.5 m. Similarly, while zero BER is recorded experimentally for LOS link up to the distance of 6 m, we observe $P_e = 8.0 \times 10^{-5}$ in the case of lateral shift. As the distance between the transmitter and receiver is increased to 8 meters, the transmission is stopped, and no packets are received after this distance.

4.3.2 With Matched Filter Bit Error Rate Measurements

In this scenario, we considering a different demodulation technique. We use the matched filter as the demodulation technique. A matched filter is a demodulation method extensively employed across diverse applications for signal detection in the presence of noise. Its operation involves creating a filter specifically tailored to the form of the transmitted or received signal. As the noisy signal undergoes the matched filter, it enhances the signal while diminishing the noise, leading to a more distinct and dependable signal.

Figure 45 illustrates the end-to-end block diagram of our experimental setup. The laptop with Vivado software generates the digital signal as the [1 0] at the transmitter side. Then, these signals are transferred to the Eclypse Z7 FPGA with Zmod 1411 daughterboard through an ethernet cable. The transmitter front-end includes a high-power LED driver and an off-the-shelf streetlight. At the receiver front-end, Thorlabs APD130A/M collects an optical signal and produces a photocurrent. The output analog signal from the photodetector is read by the ADC and transmitted digitally to the FPGA. LOS scenario was considered.In the LOS scenario, the transmitter and receiver are in perfect alignment. Figure 46 illustrates the experimental setup during measurements.

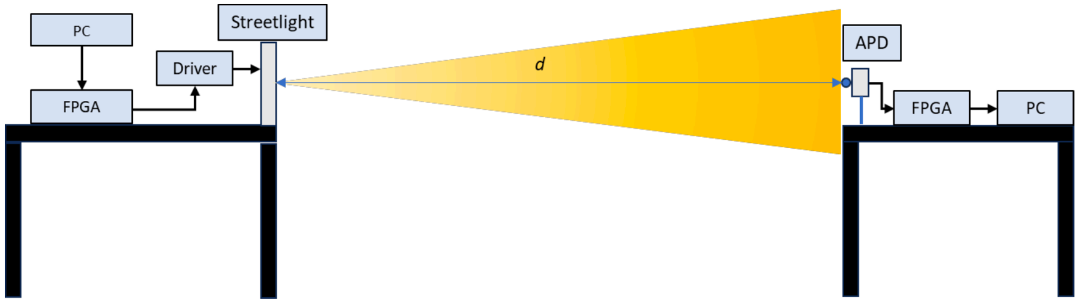

Figure 45: Block diagram of the experimental setup.

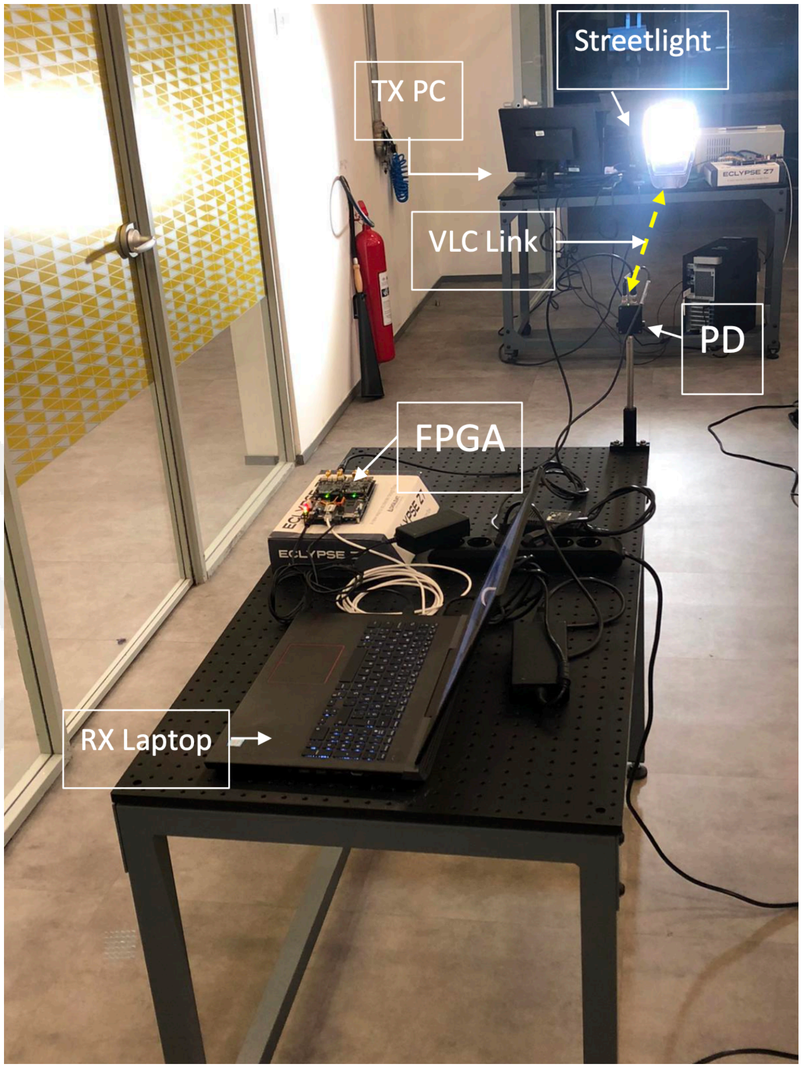

Figure 46: Experimental setup during measurements.

We send a sequence of symbols with a length of L, where symbols '0' are transmitted using even indices, and symbols '1' are transmitted using odd indices. The sequence is then directed to the streetlight, where it is transformed into optical power. A photodetector on the receiver side captures the received signal and converts it into electrical signals. The received signals at even and odd indices can be written respectively as

$$x_{\mathrm{Z}}(i) = V_{\mathrm{DC}} + w_g(i), i = 0, 2, 4..., L \tag{4.1}$$

$$x_{O}(i)=\sqrt{P_R}+V_{DC}+w_g(i), i=1,3,5...,L \tag{4.2}$$

where V_{DC} and $w_g(i)$ represent, background DC and the i^{th} sample of the Additive White Gaussian Noise (AWGN), respectively. In Equation (4.2), P_R is the electrical power of the ON state. It should be however noted that the average AC power, taking into account ON and OFF states, is $P_R/2$.

For DC-bias estimation, we take the expectation Equation (4.1) on the previous page. Mathematically speaking,

$$\begin{aligned}\widehat{V_{DC}} &= \mathrm{E}\left[\mathrm{V_{DC}}+\mathrm{w_g}\right] \\ &= \mathrm{E}\left[\mathrm{V_{DC}}\right]+\mathrm{E}\left[\mathrm{w_g}\right]\end{aligned} \tag{4.3}$$

The next step is to remove the DC from both equations of Equation (4.1) on the preceding page and Equation (4.2). Mathematically speaking, we can write

$$x_{Z,DC}(i)=\left(V_{DC}-\widehat{V_{DC}}\right)+w_g(i) \tag{4.4}$$

$$x_{O,DC}(i)=\sqrt{P_R}+\left(V_{DC}-\widehat{V_{DC}}\right)+w_g(i) \tag{4.5}$$

It is obvious that the only random variable in the previous two equations is the noise. Indicating that the variance gave us the noise power. Mathematically speaking, we can write

$$\widehat{\sigma_n^2}=\mathrm{Var}\left[\mathrm{x_{Z,DC}}\right] \tag{4.6}$$

Utilizing Equation (4.5), under the assumption of complete DC removal, we have

$$\begin{aligned}E\left[x_{O,DC}^2\right] &\approx E\left[\left(\sqrt{P_R}+w_g\right)^2\right] \\ &= E\left[P_R+w_g^2+2P_Rw_g\right] \\ &= E\left[P_R\right]+E\left[w_g^2\right]+2E\left[P_R\right]\cancel{E\left[w_g\right]} \\ &= \widehat{P_R}+\widehat{\sigma_n^2}\end{aligned} \tag{4.7}$$

From the previous calculation, we can simply estimated the received power as

$$\widehat{P_R} = E\left[x_{\mathrm{O,DC}}^2\right] - \widehat{\sigma_n^2} \tag{4.8}$$

Utilizing Equation (4.6) on the previous page and Equation (4.8), estimated SNR can be written as

$$\widehat{SNR} = \frac{\widehat{P_R}}{\widehat{\sigma_n^2}} \tag{4.9}$$

In Figure 47, we present the error rate versus SNR performance of our VLC system set-up. The experiments are conducted for distances from d = 9 m up to d = 14 m with 1 m intervals. For each point, the transmitted signals were collected through the Vivado software using ILA, and the error rate was computed from the received signals afterward by MATLAB. For benchmarking, we included theoretical BER of OOK, i.e., BER = $\mathrm{Q}\left(\sqrt{\mathrm{SNR}}\right)$.

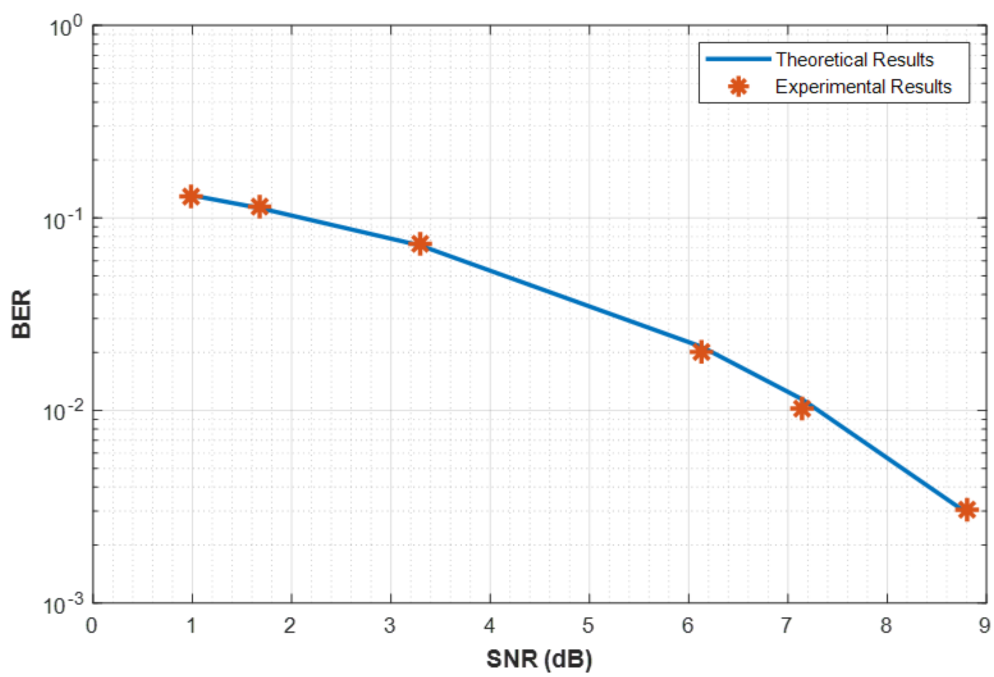

Figure 47: Theoretical and Experimental comparison of BER and SNR.

In the test scenario where there is perfect alignment between transmitter and receiver, errors were first observed at d = 9 m, and a BER of $P_e = 3.05 \times 10^{-3}$ was recorded. Similarly, while zero BER is recorded experimentally for LOS link up to the distance of 8 m, we observe $P_e = 1.29 \times 10^{-1}$ at d = 14 m. The distance between the transmitter and receiver is increased to 14 meters. The SNR value was observed as 8.80 dB at d = 9 m, and 0.98 dB at d = 14 m.

Compared with the previous scenario, Section 4.3.1, we observed a zero BER at greater distances thanks to the demodulation technique we used. We also noted a correspondence between theoretical and experimental implementation results.

4.4 Outdoor Scenarios

In this section, we discuss scenarios conducted in the outdoor environment. We observe the distance-dependent SNR performance results measured at different coordinates in the outdoor setting.

Figure 48 illustrates a VLC-based broadcasting scenario. Streetlight is utilized as wireless transmitters for broadcasting emergency and security information. In our outdoor experiment, the performance of a single streetlight is examined. The height of our streetlight from the ground is 4.5 m. As measured in Section 4.1.2, our streetlight has the power of 20 W for the optical transmission. The vehicle moves longitudinally concerning the streetlight by a distance of d_x, and it can undergo a lateral shift of d_y. The distance d_z between the photodetector and the streetlight is 3.5 m. Figure 49 illustrates the experimental setup during measurements. The outdoor experiments were conducted under clear-weather conditions during mid-day.

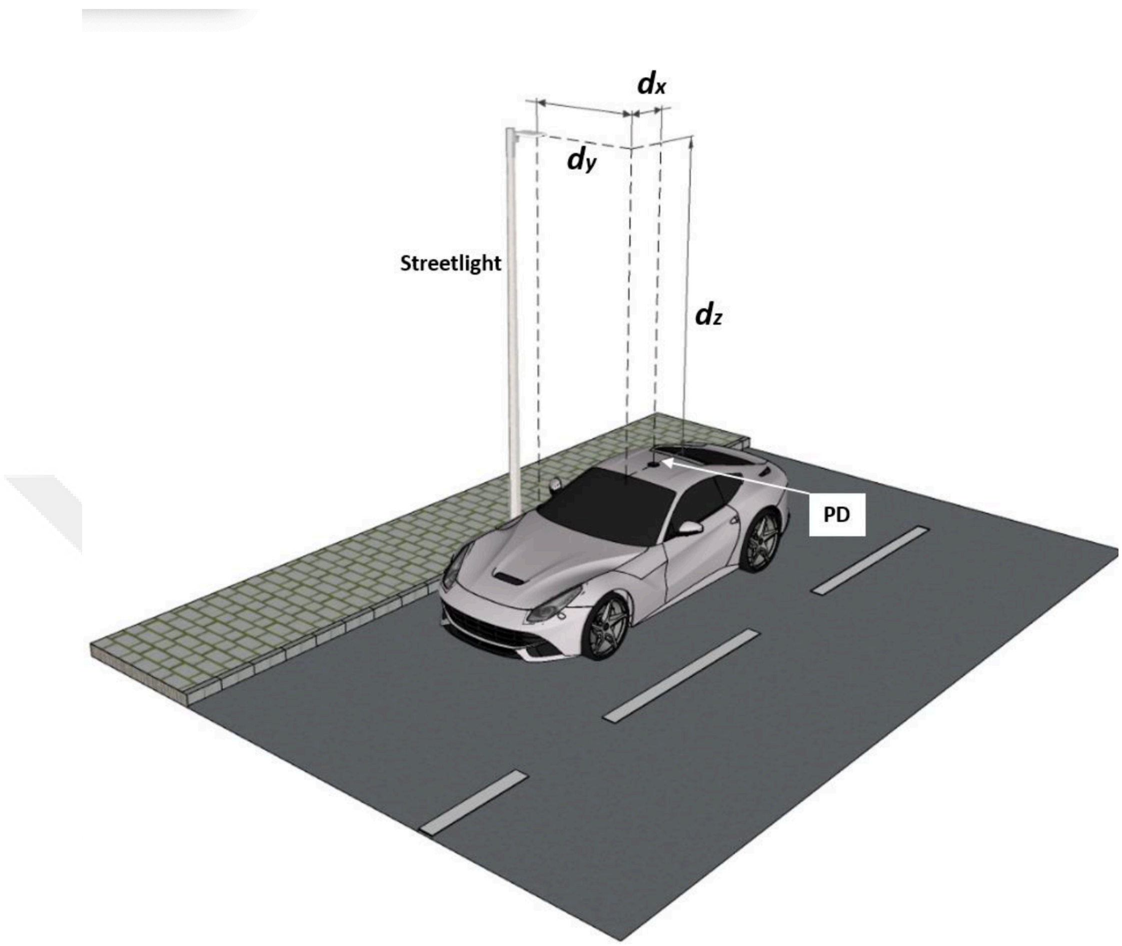

Figure 48: Outdoor VLC-based broadcasting measurements scenario.

Figure 49 illustrates the end-to-end system of our experimental setup. The signal generator generates the digital signal as the [1 0] at the transmitter side. Then, these signals are transferred to high-power LED through a cable. The transmitter front-end includes a high-power LED driver and an off-the-shelf streetlight. At the receiver front-end, Thorlabs DET36A/M [61] collects an optical signal and produces a photocurrent. The output analog signal from the photodetector is read by the ADC and transmitted digitally to the FPGA. LOS scenario was considered at $d_x = 0$ m, $d_y = 0$ m, $d_z = 3.5$ m. In the LOS scenario, the transmitter and receiver are in perfect alignment.

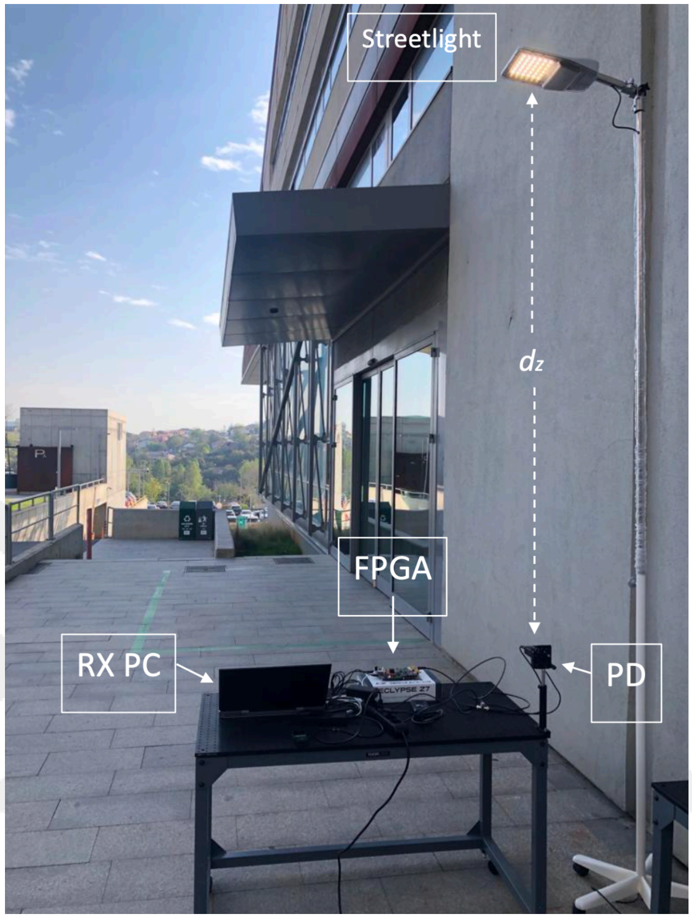

Figure 49: Experimental setup during measurements.

In Figure 50, we present the SNR performance of our VLC system setup for Streetlight-to-Vehicle (S2V) and Streetlight-to-Pedestrian (S2P) links at the different d_x points. The experiment are conducted for distances from d_x = 0 m up to d_x = 6 m with 1 m intervals in both (-6 m,6 m) directions. For each point, the transmitted signals were collected through the Vivado software using ILA. The SNR analyses have been conducted using the method outlined in Section 4.3.2.

In the test scenario, when the receiver and transmitter were in perfect alignment, we observed an SNR of 34.02 dB at d_x = 0 m. The SNR graph was observed to be symmetrical, with a 1 dB decrease observed in the first 3 meters in both (-3 m, 3 m) directions. After

d_x = 3 m, we observed a sharp decrease. When d_x = 6 m, we observed an SNR of 20.5 dB.

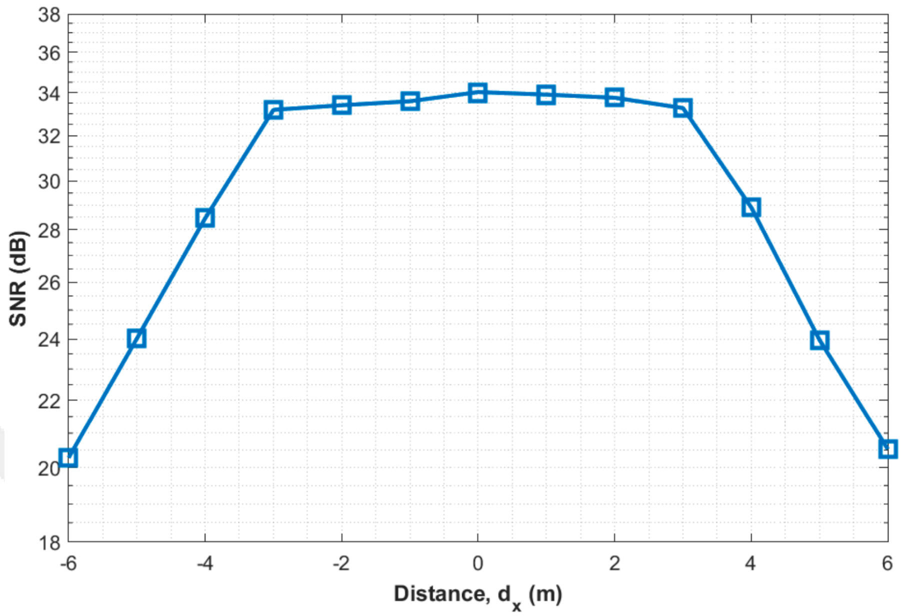

Figure 50: SNR versus distance, d_x.

In our previous scenario, we presented the SNR performance of a receiver moving longitudinally toward a streetlight. S2V links may not always follow a longitudinal path. Sometimes, vehicles may undergo lateral shifting along the road. In this scenario, we consider the impact of lateral shifting, represented by d_y, on the SNR performance of the S2V link.

In Figure 51, we present the SNR performance of our VLC system setup for S2V links at the different d_y points. The experiment is conducted for distances from d_y = 0 m up to d_y = 3 m with 1 m intervals. For each point, the transmitted signals were collected through the Vivado software using ILA. The SNR analyses have been conducted using the method outlined in Section 4.3.2.

In the test scenario, when the receiver and transmitter were in perfect alignment, an SNR of 34.02 dB is recorded at d_y = 0 m. When d_y = 1 m, d_y = 2 m and d_y = 3 m an SNR values were recorded 32.77 dB, 29.90 dB, 27.96 dB, respectively. We observed that at reduced distances, the impact of d_y is more significant. Additionally, the SNR decreases as d_y increases. The received optical power increases as the vehicle gets nearer to the streetlight.

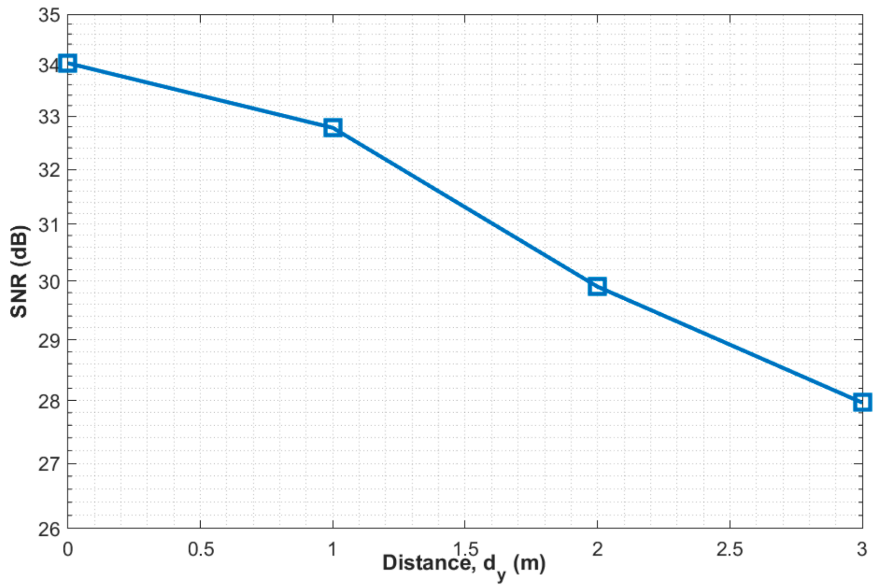

Figure 51: SNR versus distance, d_y.

In previous scenarios, we experimentally assessed the SNR performance of a receiver moving independently both longitudinally and laterally towards a streetlight, and we presented the results. However, in both scenarios, the vehicle's altitude is assumed to be the same. In vehicles with different altitudes, the SNR performance of S2V links may vary. In this scenario, we are considering the impact of altitude, represented by d_z, on the SNR performance of the S2V link.

In Figure 51, we present the SNR performance of our VLC system setup for S2V links at the different d_z points. The experiment is conducted for distances from d_z = 1.5 m up to d_z = 3.5 m with 0.5 m intervals. For each point, the transmitted signals were collected through the Vivado software using ILA. The SNR analyses have been conducted using the method outlined in Section 4.3.2.

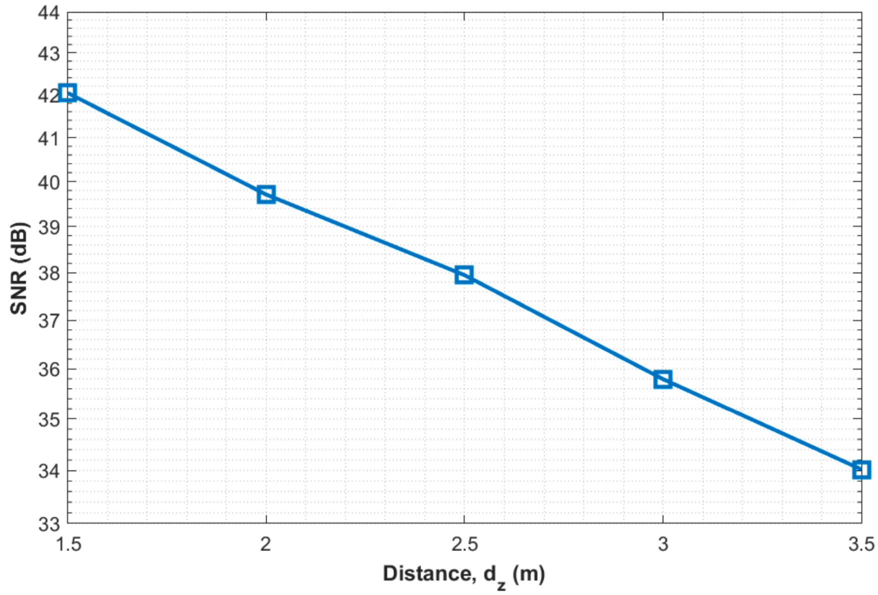

Figure 52: SNR versus distance, d_z.

In the test scenario, when the receiver and transmitter were in perfect alignment, an SNR of 42.03 dB is recorded at d_z = 1.5 m. When d_z = 2 m, d_z = 2.5 m, d_z = 3 m and d_z = 3.5 m an SNR values were recorded 39.70 dB, 37.94 dB, 35.79 dB, 34.02 dB, respectively. We observed that at greater distances, the impact of d_z is more significant. Additionally, the SNR decreases as d_z increases. The received optical power increases as the vehicle gets nearer to the streetlight.

CHAPTER V

CONCLUSION AND FUTURE WORKS

5.1 Conclusion

In this thesis, we experimentally evaluated the performance of an outdoor VLC system based on FPGA implementation. The experimental setup was built on the Eclypse Z7 FPGA with DAC and ADC expansion boards and a high-power LED driver. A commercial off-the-shelf streetlight was used as the VLC transmitter. We demonstrated that the optoelectronic front-end (i.e., that consists of the streetlight and driver) has sufficient bandwidth for broadcasting messages for public safety applications. In indoor measurements, we conducted scenarios with and without a matched filter. In the experimental setup without a matched filter, we showed that our system achieves zero BER at a distance of 6 m in LOS. Shifting the receiver front-end by 1 meter recorded zero BER at the same propagation distance of 5.5 m in NLOS. In the experimental setup with a matched filter, our BER performance showed to operate with zero BER at longer distances and matched the literature trend. In the outdoor measurements, we developed different scenarios and conducted experimental implementations. SNR performance tests were conducted for S2V and S2P links. We considered longitudinal scenarios for S2V and S2P links, as well as lateral displacement and vehicle height-dependent scenarios for S2V. After obtaining data for SNR performance tests, we analyzed and presented the data using matched filters in MATLAB. Consequently, we experimentally observed high SNR values when the BER was zero for broadcasting in public safety applications.

5.2 Future Works

In Chapter 2, we examined different types of VLC LED drivers. In Chapter 3, we designed a high-power LED driver and we operated the streetlight chosen as the transmitter. Due to the limited bandwidth of the streetlight, high-speed data communication was not feasible. As a future research work, pre-equalized can be designed to increase the system's bandwidth. As another possible direction, the multi-carrier system in the form of Orthogonal Frequency Division Multiplexing (OFDM) can be used.

In Section 4.4 we conducted measurement campaigns in outdoor scenarios with d_x, d_y, and d_z, and we presented the SNR performance results when BER is zero. Outdoor scenarios can be extended. In outdoor measurements, power measurements can be performed in d_x and d_y scenarios, proving the radiation pattern of the streetlight, or a new closed-form expression can be investigated for streetlights with asymmetric radiation patterns.

One of the hot topics in research is to use Reconfigurable Intelligent Surfaces (RISs). This can be used by different methods and for different applications. For example, it can be placed on the top of the vehicle and assist in using the vehicle as a hop to connect two streetlights. As another potential research direction is to consider employing Unmanned Aerial Vehicle s (UAVs). In this case, there could be a possible link between UAV and the streetlights.

REFERENCES

[1] M. A. Khalighi and M. Uysal, "Survey on free space optical communication: A communication theory perspective," *IEEE Communications Surveys & Tutorials*, vol. 16, no. 4, pp. 2231–2258, 2014.

[2] A. A. Huurdeman, "The worldwide history of telecommunications," in *John Wiley Hoboken, N.J*, pp. 18–26, 2003.

[3] G. J. Holzmann and B. Pehrson, "The early history of data networks (perspectives)," in *John Wiley Hoboken, N.J*, pp. 1–44, 1995.

[4] J. Hecht, "Short history of laser development," *Optical Engineering, SPIE*, vol. 49, no. 9, p. 091002, 2010.

[5] F. E. Goodwin, "A review of operational laser communication systems," *Proc. IEEE*, vol. 58, pp. 1746–1752, Oct. 1970.

[6] T. Tolker-Nielsen and G. Oppenhauser, "In-orbit test result of an operational intersatellite link between artemis and spot 4," in *Proc. SPIE, Free-Space Laser Commun. Technol. XIV*, vol. 4639, (San Jose, CA, USA), pp. 1–15, Jan. 2002.

[7] R. Lange, B. Smutny, B. Wandernoth, R. Czichy, and D. Giggenbach, "142 km, 5.625 gb/s free-space optical link based on homodyne bpsk modulation," in *Proc. SPIE, Free-Space Laser Commun. Technol. XVIII*, vol. 6105, p. 61050A, 2006.

[8] B. Smutny *et al.*, "5.6 Gbps optical intersatellite communication link," in *Proc. SPIE, Free-Space Laser Commun. Technol. XVIII*, vol. 7199, p. 719906, Feb. 2009.

[9] N. Karafolas and S. Baroni, "Optical satellite networks," *J. Lightw. Technol.*, vol. 18, pp. 1792–1806, Dec. 2000.

[10] European Data Relay System (EDRS). `http://www.esa.int/Our_Activities/Telecommunications_Integrated_Applications/EDRS`. [Online, Accessed: January 15, 2024].

[11] H. Hemmati, "Deep space optical communications," in *John Wiley Hoboken, N.J*, pp. 1–82, 2006.

[12] Laser Comm: That's a Bright Idea. `http://svs.gsfc.nasa.gov/vis/a010000/a011000/a011036/`. [Online, Accessed: January 15, 2024].

[13] S. Dimitrov and H. Haas, "Principles of led light communications: Towards networked li-fi," in *Cambridge University Press*, pp. 1–11, 2015.

[14] F. Miramirkhani and M. Uysal, "Channel modeling and characterization for visible light communications," *IEEE Photonics Journal*, vol. 7, no. 6, pp. 1–16, 2015.

[15] X. Wu, M. D. Soltani, L. Zhou, M. Safari, and H. Haas, "Hybrid lifi and wifi networks: A survey," *IEEE Communications Surveys & Tutorials*, vol. 23, no. 2, pp. 1398–1420, 2021.

[16] A. Memedi and F. Dressler, "Vehicular visible light communications: A survey," *IEEE Communications Surveys & Tutorials*, vol. 23, no. 1, pp. 161–181, 2021.

[17] A.-M. Căilean and M. Dimian, "Current challenges for visible light communications usage in vehicle applications: A survey," *IEEE Communications Surveys & Tutorials*, vol. 19, no. 4, pp. 2681–2703, 2017.

[18] F. S. Diana, G. Guth, J. Den Breejen, and I. Black, "Asymmetrical light intensity distribution from luminaire," Sep. 2019. U.S. Patent.

[19] H. B. Eldeeb, M. Elamassie, S. M. Sait, and M. Uysal, "Infrastructure-to-vehicle visible light communications: Channel modelling and performance analysis," *IEEE Transactions on Vehicular Technology*, vol. 71, no. 3, pp. 2240–2250, 2022.

[20] J.-H. Lee and S.-Y. Jung, "Snr analyses of the multi-spectral light channels for optical wireless led communications in intelligent transportation system," in *2014 IEEE 79th Vehicular Technology Conference (VTC Spring)*, pp. 1–5, 2014.

[21] S. Lee, J. K. Kwon, S.-Y. Jung, and Y.-H. Kwon, "Evaluation of visible light communication channel delay profiles for automotive applications," *Eurasip J. Wireless Commun. Netw.*, vol. 2012, p. Art. no. 370, Dec. 2012.

[22] M. S. Demir, H. B. Eldeeb, and M. Uysal, "Comp-based dynamic handover for vehicular vlc networks," *IEEE Communications Letters*, vol. 24, no. 9, pp. 2024–2028, 2020.

[23] M. S. Demir, H. B. Eldeeb, and M. Uysal, "Relay-assisted handover technique for vehicular vlc networks," *IEEE Access*, vol. 10, pp. 87387–87398, 2022.

[24] V. Georlette, S. Bette, S. Brohez, R. Pérez-Jiménez, N. Point, and V. Moeyaert, "Outdoor visible light communication channel modeling under smoke conditions and analogy with fog conditions," *Optics*, vol. 1, pp. 259–281, 2020.

[25] T. H. Do and M. Yoo, "Visible light communication based vehicle positioning using led street light and rolling shutter cmos sensors," *Optics Communications*, vol. 407, pp. 112–126, 2018.

[26] F. Knobloch, "Channel gain and frame error rate for optical street lighting communication," in *2015 13th International Conference on Telecommunications (ConTEL)*, pp. 1–5, 2015.

[27] F. Knobloch, "Impact of dimming and aperture on the optical wireless performance in public street lighting," in *2017 14th International Conference on Telecommunications (ConTEL)*, pp. 27–34, 2017.

[28] R. S. Sitanggang, D. Darlis, and K. W. Noviyanti, “Performance of outdoor lamp implementation for visible light communication under ambient environment,” *Journal of Physics: Conference Series*, vol. 1364, p. 012008, Dec. 2019.

[29] Digilent. `https://media.digikey.com/pdf/Data%20Sheets/Digilent%20PDFs/410-393_Web.pdf`. [Online, Accessed: January 15, 2024].

[30] L. Teixeira, F. Loose, C. H. Barriquello, V. A. Reguera, M. A. D. Costa, and J. M. Alonso, “A review of led drivers for visible light communication,” in *IECON 2019 - 45th Annual Conference of the IEEE Industrial Electronics Society*, vol. 1, pp. 4274–4279, 2019.

[31] ENERGY STAR, “ENERGY STAR Program Requirements for Computers Partner Commitments for Lamps (Light Bulbs).” . `https://www.energystar.gov/sites/default/files/specs//Version61ComputersFinalProgramRequirements.pdf`. [Online, Accessed: January 15, 2024].

[32] J. M. Alonso, D. Gacio, A. J. Calleja, F. Sichirollo, M. F. da Silva, M. A. D. Costa, and R. N. do Prado, “Reducing storage capacitance in off-line led power supplies by using integrated converters,” in *2012 IEEE Industry Applications Society Annual Meeting*, pp. 1–8, 2012.

[33] X. Deng, Y. Wu, K. Arulandu, G. Zhou, and J.-P. M. G. Linnartz, “Performance comparison for illumination and visible light communication system using buck converters,” in *2014 IEEE Globecom Workshops (GC Wkshps)*, pp. 547–552, 2014.

[34] J. Sebastián, D. G. Lamar, D. G. Aller, J. Rodríguez, and P. F. Miaja, “On the role of power electronics in visible light communication,” *IEEE Journal of Emerging and Selected Topics in Power Electronics*, vol. 6, no. 3, pp. 1210–1223, 2018.

[35] J. Sebastián, P. Fernández-Miaja, F. J. Ortega-González, M. Patiño, and M. Rodríguez, “Design of a two-phase buck converter with fourth-order output filter for envelope amplifiers of limited bandwidth,” *IEEE Transactions on Power Electronics*, vol. 29, no. 11, pp. 5933–5948, 2014.

[36] X. Deng, K. Arulandu, Y. Wu, G. Zhou, and J.-P. M. G. Linnartz, “Performance analysis for joint illumination and visible light communication using buck driver,” *IEEE Transactions on Communications*, vol. 66, no. 5, pp. 2065–2078, 2018.

[37] S. Zong, J. Wu, and X. He, “A novel method for illumination and communication using white led lights,” in *6th IET International Conference on Power Electronics, Machines and Drives (PEMD 2012)*, pp. 1–5, 2012.

[38] F. Loose, R. R. Duarte, C. H. Barriquello, M. A. Dalla Costa, L. Teixeira, and A. Campos, “Ripple-based visible light communication technique for switched led drivers,” in *2017 IEEE Industry Applications Society Annual Meeting*, pp. 1–6, 2017.

[39] J. Rodriguez, D. G. Lamar, J. Sebastian, and P. F. Miaja, “Taking advantage of the output voltage ripple of a two-phase buck converter to perform quadrature amplitude modulation for visible light communication,” in *2017 IEEE Applied Power Electronics Conference and Exposition (APEC)*, pp. 2116–2123, 2017.

[40] F. Loose, L. Teixeira, R. R. Duarte, M. A. Dalla Costa, and C. H. Barriquello, “On the use of the intrinsic ripple of a buck converter for visible light communication in led drivers,” *IEEE Journal of Emerging and Selected Topics in Power Electronics*, vol. 6, no. 3, pp. 1235–1245, 2018.

[41] J. Rodríguez Mendez, D. G. Lamar, D. G. Aller, P. F. Miaja, and J. Sebastián, “Reproducing multicarrier modulation schemes for visible light communication with the ripple modulation technique,” *IEEE Transactions on Industrial Electronics*, vol. 67, no. 2, pp. 1532–1543, 2020.

[42] T. Kishi, H. Tanaka, Y. Umeda, and O. Takyu, “A high-speed led driver that sweeps out the remaining carriers for visible light communications,” *Journal of Lightwave Technology*, vol. 32, no. 2, pp. 239–249, 2014.

[43] H. Tanaka, Y. Umeda, and O. Takyu, “High-speed led driver for visible light communications with drawing-out of remaining carrier,” in *2011 IEEE Radio and Wireless Symposium*, pp. 295–298, 2011.

[44] National Instrument. `https://www.ni.com/en-tr/shop/wireless-design-test/what-is-a-usrp-software-defined-radio/what-is-ni-usrp-hardware-.html`. [Online, Accessed: January 15, 2024].

[45] Field Programmable Gate Array. `https://en.wikipedia.org/wiki/Field-programmable_gate_array`. [Online, Accessed: January 15, 2024].

[46] Eclypse Z7 SoC Development Board with SYZYGY-compatible Expansion. `https://www.xilinx.com/products/boards-and-kits/1-18tmbd2.html`. [Online, Accessed: January 15, 2024].

[47] Microcontroller. `https://en.wikipedia.org/wiki/Microcontroller`. [Online, Accessed: January 15, 2024].

[48] Arduino. `https://store.arduino.cc/products/arduino-uno-rev3`. [Online, Accessed: January 15, 2024].

[49] H. Haugan, S. Elhamri, F. Szmulowicz, B. Ullrich, G. Brown, and W. Mitchel, “Study of residual background carriers in midinfrared inas/gasb superlattices for uncooled detector operation,” *Applied Physics Letters - APPL PHYS LETT*, vol. 92, pp. 1102–071102, 02 2008.

[50] What is the Difference Between a PIN Photodiode and a PN Photodiode? `https://www.neoncq.com/what-is-the-difference-between-a-pin-photodiode-and-a-pn-photodiode.html`. [Online, Accessed: January 15, 2024].

[51] Phototransistor. https://electronicscoach.com/phototransistor.html. [Online, Accessed: January 15, 2024].

[52] Photomultiplier tube. https://en.wikipedia.org/wiki/Photomultiplier_tube. [Online, Accessed: January 15, 2024].

[53] Photodiode. https://www.electricaltechnology.org/2022/07/photodiode.html. [Online, Accessed: January 15, 2024].

[54] "CCD vs CMOS." https://www.rfwireless-world.com/Terminology/CCD-vs-CMOS.html. [Online, Accessed: January 15, 2024].

[55] EPC. https://epc-co.com/epc/Portals/0/epc/documents/datasheets/EPC2052_datasheet.pdf. [Online, Accessed: January 15, 2024].

[56] Texas Instrument. https://www.ti.com/product/LMG1020?HQS=TI-null-null-octopart-df-pf-manuf-wwe. [Online, Accessed: January 15, 2024].

[57] PELSAN. https://pelsan.com.tr/madrid-yol-ve-cadde-armaturleri. [Online, Accessed: January 15, 2024].

[58] Thorlabs. https://www.thorlabs.com/thorproduct.cfm?partnumber=APD130A/M. [Online, Accessed: January 15, 2024].

[59] VISO. https://www.visosystems.com/special/. [Online, Accessed: January 15, 2024].

[60] LapSpion. https://www.visosystems.com/products/labspion/. [Online, Accessed: January 15, 2024].

[61] Thorlabs. https://www.thorlabs.com/thorproduct.cfm?partnumber=DET36A/M. [Online, Accessed: January 15, 2024].

VITA

İbrahim Bağlıca is an Optical Engineer currently working as an Optical Systems Engineer at Hyperion Technologies. He received his B.Sc. in Optic & Acoustic Engineering from Gaziantep University, Gaziantep, Turkey, in 2020. He is currently pursuing an M.Sc. degree in the Electrical & Electronics Engineering department under the supervision of Prof. Murat Uysal at Ozyegin University, Istanbul, Turkey. During his graduate studies, he worked at the OKATEM laboratory at Ozyegin University. His current research interests include optical wireless communication, visible light communication, and experimental communication system design in optical fields.